Doctoral Dissertation

(Shinshu University)

Study on photo-reduced molybdenum oxide polyacrylonitrile composite membranes for modern dressing materials

FAROOQ MUHAMMAD

March 2024

Graduate School of Medicine, Science and Technology

Shinshu University

信州大学審査学位論文

光還元モリブデン酸化物ポリアクリロニトリル複合膜の近代的ドレッシング材への応用に関する研究

ファルーク　ムハンマド

2024 年　3 月

信州大学繊維学部　総合医理工学研究科　総合理工学専攻

Doctoral Dissertation Evaluation Committee

Chairperson: Prof. Ick Soo Kim

Examiner: Dr. Chunhong ZHU

Examiner: Dr. Jian Shi

Examiner: Prof. Hyung Joon CHA (Department of Chemical Engineering, Pohang University of Science and Technology, Pohang, Korea

博士学位論文審査委員会

主査： 翼水金 教授

副査： 朱 春紅 (准教授)

副査： 施 建 (准教授)

外部委員： Prof. Hyung Joon CHA (Department of Chemical Engineering, Pohang University of Science and Technology, Pohang, Korea

CONTENTS

Abstract:

In this study, the research focuses on developing modern wound dressings materials using molybdenum oxide and polyacrylonitrile support material. First phase we evaluate the effects of various reducing agents for the synthesis of silver nanoparticles on the surface of MoO_3 nanoparticles deposited PAN nanofiber membrane and further study their properties The nanofibers were treated with NaOH, $NaBH_4$, sodium citrate, and UV, leading to different outcomes in terms of surface wettability, antibacterial properties, and silver ion release. The surface wettability of the nanofibers varied with the treatment. NaOH treatment reduced surface wettability, while $NaBH_4$ and sodium citrate treatments increased it. UV treatment resulted in a slight increase in surface wettability. Antibacterial inhibition zone tests revealed that NaOH and UV treatments exhibited significant inhibitory effects against both *E. coli* and *B. subtilis* bacteria, whereas $NaBH_4$ and sodium citrate treatments displayed moderate inhibitory effects. Furthermore, the study explored the sustained release of silver ions over time, with sodium citrate treated samples t exhibiting a higher release rate. While the addition of molybdenum oxide nanoparticles into the PAN nanofiber substantially lower stress values, which is advantageous for wound dressings, as it allows for improved flexibility and conformability to the wound site.

Now we fully understand the effects of different reducing agents for the reduction of silver ions to metallic silver on MoO_3np containing PAN nanofibers. Moving on, our study focused on the development of hybrid composite material with the use of molybdenum oxide and polyacrylonitrile support. For the very first time we successfully synthesized MoO_3/PAN composite material with electrospinning setup. The synthesis of Ag@MoO_3/PAN involved fast eco-friendly method under UV light (for 1 mints) for the reduction of silver ions to metallic silver on the surface of MoO_3/PAN composite membrane. The setup was very easy and industrial scale synthesis being also possible. This hybrid material not only overcame the challenge of excessive release of silver from nanofiber matrix, but also eliminated other toxic reducing agents for the synthesis of silver nanoparticles on nanofiber membranes. In the first half research highlighted the morphological characteristics and structural attributes of the synthesized composite membranes. Additionally, we investigated the antibacterial mechanisms of both Mo based nanofiber membrane and silver doped based membrane., revealing that the incorporation of silver substantially enhanced antibacterial activity. The study further elucidated the surface properties of the composite membrane, noting that the introduction of silver increased the surface area by 25.89% compared to the pristine MoO_3/PAN membrane. It also observed a 9% reduction in the water contact

angle (WCA) for the Ag@MoO_3/PAN membrane, indicating improved hydrophilicity. Further we examine the release behavior of the silver ions form Ag@MoO_3/PAN membrane. Our findings demonstrate an initial burst in silver release of about 70% within the first 7 hours, followed by a 33.52% reduction and then a sustained release pattern over a period of 7 days. The mitigation of excessive silver was because of molybdenum oxide absorption mechanism for silver ions. This composite membrane dressing helps for sustained release of silver near wound site and protect the skin from damage of excessive silver release.

We believe that our study not only holds promise for extensive research in the realm of different reducing and their effects on silver nanoparticles synthesis with silver release and antimicrobial activity we also controlling the release behavior of silver ions from wound dressing by composite material method.

CHAPTER 1. General Introduction

1.1 Electrospinning technique for nanofiber synthesis

1.2 Electrospinning technique

Electrospinning is presently the sole method allowing the synthesis of continuous fibers with tiny diameters, as small as a few nanometers. This technique can be applied to various materials, including man-made and natural polymers, polymer mixtures, and polymers infused with color molecules, very small particles, or active substances. It's also compatible with metals and ceramics[1]. Special electrospinning techniques enable the production of intricate fiber structures, such as core-shell or hollow fibers. Moreover, it's feasible to produce structures ranging from individual fibers to well-organized arrays of fibers[21]. Electrospinning is not confined to academic research but is increasingly used in industry as well. Its range of applications spans a wide spectrum of fields, including optoelectronics, sensor technology, catalysis, filtration, medicine, biotechnology, and wound dressings. These applications yield materials composed of fibers so delicate that they cannot be observed even with the most advanced optical microscopes[3]. They encompass tissues made of fibers thinner than what the finest optical microscope can detect, polymer webs on plants finer than spiderwebs, filters covered by an almost imperceptible layer, greatly enhancing their efficiency and wound dressings. In fact, electrospun fibers are notably thinner than human hair. **Figure *1—1*** illustrates the number of scientific publications and patents with keywords electrospinning.

Today, nanofibers from synthetic or natural polymers can be fabricated in a controlled manner with dimensions down to a few nanometers and functionalized by the addition of drugs, or of semiconductor or catalyst nanoparticles. They can be employed in numerous applications with great benefit. Hybrid fibers composed of metals and ceramics are attainable, as are nanofibers with a solid or liquid core and a solid shell[4].

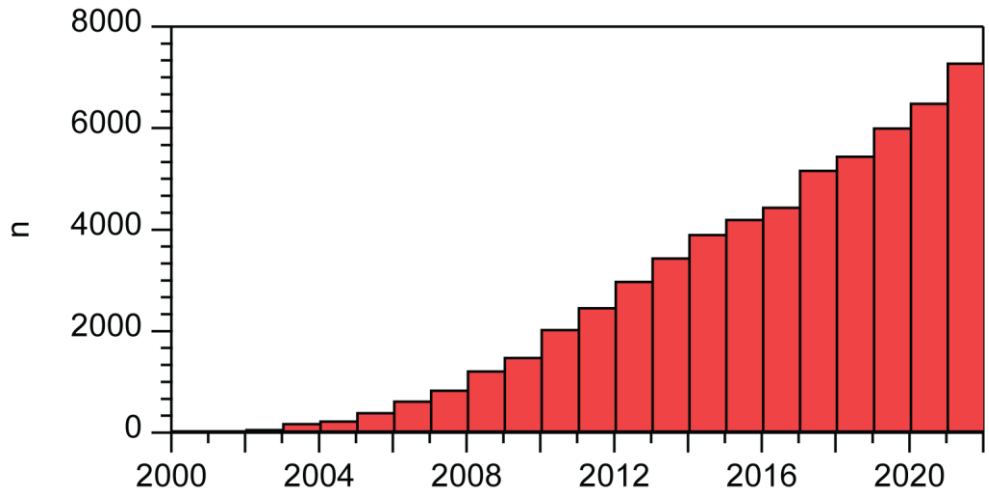

Figure 1—1: Number (n) of scientific publications and patents per year (2000–2022) with the keyword “electrospinning” (source: SciFinder Scholar)

1.3 Electrospinning history and setup

Electrospinning, also referred to as electrostatic spinning, has its roots in early studies. As far back as 1745, Bose described the creation of tiny droplets by applying high electrical potential to liquid drops. In 1882, Lord Rayleigh delved into the question of how many charges were necessary to overcome the surface tension of a droplet. Later, the initial devices designed to disperse liquids using an electric charge were patented by Cooley and Morton in 1902 and 1903. In 1929, Hagiwara et al. documented the production of artificial silk through the application of electrical charge. The pivotal patent that first described the electrospinning of plastics emerged in 1934, with Anton Formhals from Mainz as the author (originally stemming from a German patent submission in 1929)[5].

Despite these early revelations, the process was not put to commercial use. It wasn't until the 1970s that Simm et al. patented the production of fibers with diameters less

than 1mm. Nevertheless, this work, along with subsequent patents, went largely unnoticed[6]. The first commercial application of electrospun fibers was in the field of filters, as part of the nonwoven industry. The electrospinning setup that was used in our research work is described in **Figure *1—2***.

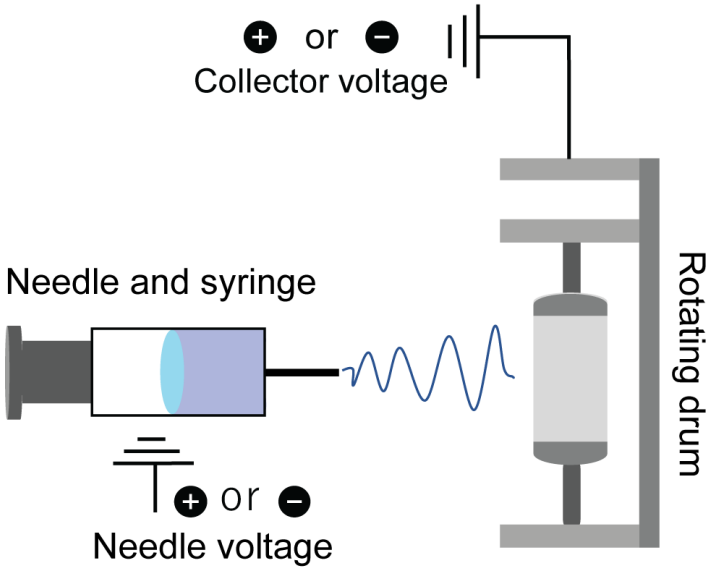

Figure 1—2: Schematic illustration of electrospinning setup for nanofiber synthesis

1.4 Skin wound and types.

The skin serves as our protective barrier against germs and infections. When the skin gets damaged due to accidents, it can lead to the formation of wounds. Depending on the nature of the accidents, circumstances, and the severity of the injury, wounds can be categorized into various types, ranging from minor to moderate to severe wounds, from small to large wounds, from superficial to deep wounds, and from non-infectious to infectious wounds[7,8]. These injuries can include burns, bruises, cuts from knives, crushing injuries, puncture wounds, and gunshot wounds. They can also be classified as acute wounds, which occur suddenly and heal quickly, such as minor scrapes, knife cuts, minor burns, or wounds right after surgery. On the other hand, chronic wounds, such as

ulcers, diabetic foot ulcers, venous leg ulcers, arterial leg ulcers, chronic radiation injuries, and deep burns or scalds, have a much longer healing process[9].Different types of wounds that occurred during the minor injuries were represented in **Figure *1—3***.

Regardless of the type of injury or trauma, if germs manage to breach the skin, it becomes necessary to clean and remove any dirt or contaminants from the wound. It is vital to sterilize and cover the wound to prevent infection and inflammation[9,10].

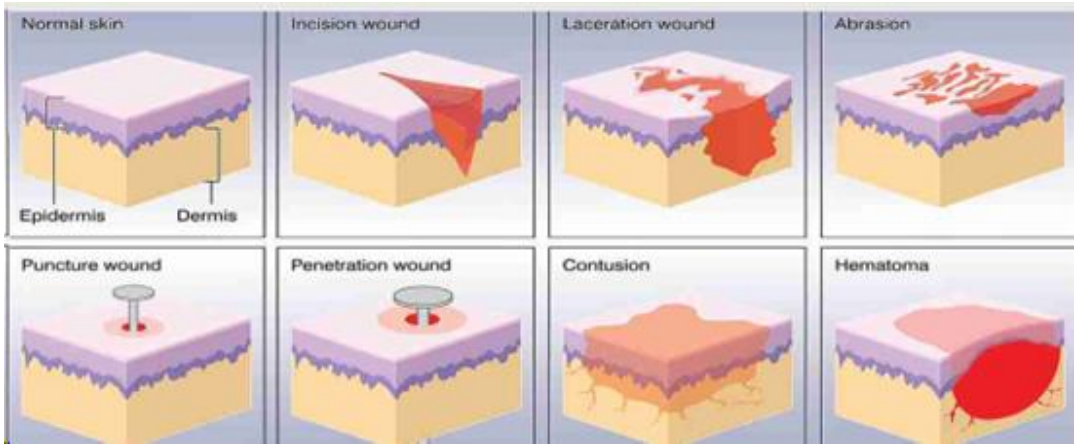

Figure 1—3: Wound types on human body skin.

It is necessary to treat and monitor the wounds if they are bleeding, large, deep, or infectious. Particularly, the application of wound dressings plays a very critical role in wound healing and infectious prevention. There are many different types of wound dressings such as silver-containing hydrophilic fiber dressing, antibacterial dressing, and wet dressing. Based on different materials, they can be classified as foams gauze, transparent films, alginates, composites, hydrocolloids, and hydrogel. Meanwhile, a good dressing with high quality and ideal function will speed up wound healing, reduce patients' pains, and prevent wounds from germ infection[11–15].

1.5 Wound healing process

The process of healing wounds is complex, and there are different ways to treat different types of wounds. Depending on where the injury is, whether it's infected, and what medical treatments are needed, we can divide wound healing into three main categories: primary healing, secondary healing, and subeschar healing[16–18].Graphical represented in **Figure *1—4***. Primary healing happens when wounds are small, have clean edges without infection, and are carefully stitched up, so they come together neatly. A typical example of primary healing is when a surgical incision heals. While secondary healing often occurs in larger wounds with more tissue damage, irregular edges, or infection by germs. These wounds heal by filling in the damaged tissue with granulation tissue, and it's also called indirect wound healing. Inflammation is more noticeable during secondary healing due to ongoing germ infection and tissue death. Normally, tissue starts to grow back once the germ infection is controlled, and the dead tissue is removed. Secondary healing is characterized by a larger wound area, noticeable shrinkage, a longer healing process, and more scar tissue formation[1920]. The blood, fluid, or dead tissue on the wound's surface dries up and forms a scab. In cases where there's no infection, wound healing can take the form of subeschar healing. In subeschar healing, new skin grows beneath the scab from the edges of the wound, covering the original connective tissue on the wound's surface or the new connective tissue filling the gaps in the skin[1021]. The scab falls off once the new skin has fully grown. Eschars are usually dry and can prevent germs from growing, offering some protection to the wound and aiding in wound healing. However, if there's too much fluid or germ infection beneath the scab, it can block the natural drainage of the wound and hinder the healing process. So far, to improve dressing antimicrobial properties different agents have been

incorporated within their structure[22]. Those antimicrobial agents comprise essentially antibiotics (e.g. tetracycline, ciprofloxacin, gentamicin and sulfadiazine), nanoparticles (e.g. silver and copper nanoparticles) and natural products (e.g. honey, essential oils and chitosan)[13,23–28]

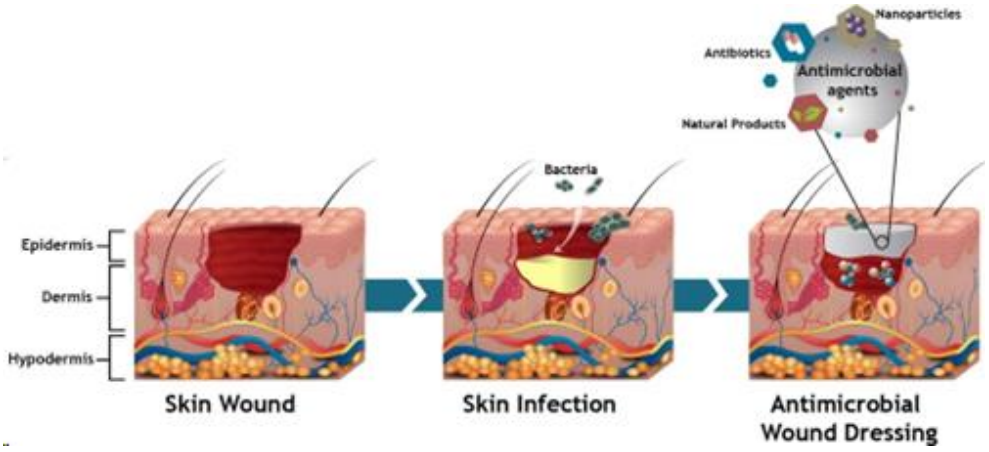

Figure 1—4: A graphical representation of skin wound, skin infection, and antimicrobial wound dressing on skin wound. Reprinted with permission from reference. [22] Copyright 2018 Elsevier-EJPB

1.6 Types of wound dressing

Wound dressings are essential in treating wounds effectively. A suitable dressing can aid in the healing of wounds and prevent infection by germs. Furthermore, it's often necessary to switch between various types of wound dressings throughout the entire treatment process. Sometimes, different dressings may even need to be used together to create a favorable environment for wound recovery and protection. During wound treatment, there are several types of dressings available, including foams, gauze, transparent films, alginates, composites, hydrocolloids, and hydrogel[22,24,29–31]. Each dressing has its unique characteristics, as outlined in **Table 1**.

Table 1:Types of wound dressing and characteristics

Types	Characteristics
Foams	Foam dressings are commonly created from polyurethane foam and are typically applied to moderate to severe wounds. These dressings provide a soft and cushioning effect while effectively soaking up a significant amount of wound exudate. They possess excellent absorption capabilities, creating a moist and warm environment conducive to wound healing.
Gauze	Gauze dressings are a classic kind of wound dressing manufactured from woven cotton or synthetic fibers. They are adaptable, cost-effective, and easily accessible, making them a widely chosen option for wound treatment.
Transparent membrane	Transparent film dressings are thin, see-through, and waterproof. They enable the observation of wounds without the need to take off the dressing. These dressings are typically created from polymer membranes that permit oxygen to access the wound while letting vapor escape
Alginates	Alginate dressings are crafted from seaweed and consist of calcium and sodium ions. When these dressings encounter a wound, they form a gel-like substance.
Composites	Composite wound dressings are a specific type of dressing that blends various materials like foam, hydrocolloid, and alginate into one dressing. These dressings are created to offer a mix of advantages, including absorption, moisture regulation, and protection. They are frequently employed in the treatment of intricate wounds.
Hydrocolloids	Hydrogel mixed with synthetic rubber and sticky materials, has excellent exudate absorption properties.
Silver dressing	Silver wound dressings include silver, a natural antimicrobial substance that can assist in preventing and treating wound infections. These dressings can encompass silver in various formats, including ions. particles, or compounds, and come in various forms, such as gels, foams, and films.

1.7 Metal-based antibacterial wound dressing

Humans face threats from bacteria and various microorganisms that lead to numerous infections and illnesses every year. It's important to note that since the introduction of the last new class of antibiotics in 2003, treating many infectious diseases has become increasingly challenging, especially those caused by bacteria resistant to multiple drugs[3233]. The Centers for Disease Control and Prevention (CDC) in the US estimated that globally, over 2 million infections and nearly 30,000 deaths occur annually due to antibiotic resistance[34]. There is an urgent need for new strategies to combat microbial infections, given the growing challenges associated with the post-antibiotic era. In this era, infections that were once responsive to antibiotics have developed resistance to even the most contemporary antibiotic classes[35]. Biomedical devices that incorporate antimicrobial metal nanostructures present a promising approach to combating these extensively drug-resistant pathogens[36,37]. These devices have garnered significant attention in both academic and pharmaceutical circles. Different mechanisms are employed by these antimicrobial metal nanostructures, and they offer a potential solution to the growing problem of drug-resistant infections[38–40]. To prevent redundancy, metal nanoparticles are utilized as representatives to symbolize all antibacterial materials[41–43]. Subsequently, a concise overview of the antiviral and antifungal mechanisms of nanomaterials will follow.

1.8 Bacterial cells and death of bacteria

Bacterial structure consists of fundamental components, including the cell wall, cell membrane, nucleoid, and cytoplasm, which houses ribosomes and plasmids. In contrast to Gram-negative bacteria, Gram-positive bacteria possess an additional layer known as the peptide cross-bridge[44]. Another distinguishing feature of Gram-positive bacteria is

the presence of teichoic acid. Teichoic acid is connected to the cell wall or cell membrane through covalent bonds, specifically wall teichoic acid and lipoteichoic acid. In the case of Gram-negative bacteria, the outer membrane is the predominant characteristic[45,46]. In terms of antibacterial mechanisms related to bacterial cell walls, electrostatic interaction plays a critical role. These surfaces carry a negative charge, which facilitates the adhesion of positively charged materials like Ag or Al_2O_3 nanoparticles. Nanogel particles can bind to proteins in the bacterial cell wall containing sulfur or phosphorus[47–49]. This interaction leads to the formation of enhanced nanopores on the cell wall, ultimately resulting in the death of the bacterial cell. Reactive oxygen species generated by metallic nanomaterials can also directly disrupt the components inside the bacterial cytoplasm[50]. A notable example is the damage to DNA caused by these reactive oxygen species within the nucleoid. Silver ions, for instance, can disrupt the hydrogen bonds between the two antiparallel polynucleotide strands, potentially leading to DNA denaturation[51]. Additionally, nanoparticles can intercalate between the purine and pyrimidine base pairs, further contributing to DNA changes. Nanoparticles possess a high absorption capacity, which can influence signal transduction in bacteria through protein phosphorylation[35]. They have been observed to dephosphorylate peptide substrates on tyrosine residues, leading to the inhibition of signal transduction and the arrest of cell growth and cell cycle progression[52,53].Represented in **Figure *1*—*5***.

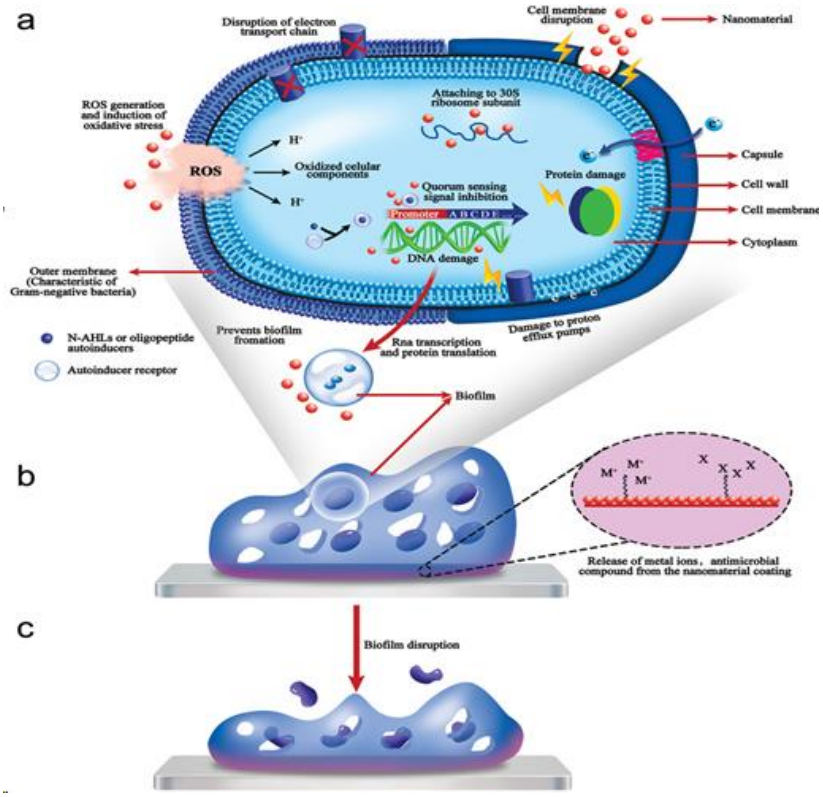

Figure 1—5: The different antibacterial mechanisms associated with the use of nanomaterials. Reprinted with permission from reference. [52] Copyright 2023 ACS-Appl Nano Mater

1.9 Silver-doped and Copper-doped antibacterial mechanism.

The biological effects of nano silver are mainly attributed to the presence of silver cations and their soluble complexes. Additionally, particle surface reactions can contribute by generating reactive oxygen species (ROS) or catalyzing the oxidation of cellular components. Silver ions bind to thiol groups in biological enzymes, such as NADH dehydrogenase, disrupting the bacterial respiratory chain and producing ROS, leading to oxidative stress and cell damage[46,54,55]. Nano silver particles have been observed to create peroxide intermediates during reactive dissolution, which may oxidize lipids when the particles attach to cell membranes. It is widely agreed that the

release of silver ions is a significant pathway for the biological activity of nanosilver[56,57].There have been research studies on the release of silver from silver-polymer composites, but there is a lack of comprehensive systematic studies on the controlled release chemistry for colloidal nano silver surfaces. There were also issues with the excessive silver release that damaged the human cells and harmed the environment[22,58,59].

While the precise antibacterial mechanism of silver-based nanomaterials hasn't been fully elucidated, the scientific community has reached several widely accepted conclusions. Generally, AgNPs (silver nanoparticles) could kill bacteria by themselves. However, numerous studies have demonstrated that the silver ions released from these particles play a more significant role in bacterial eradication[60–62]. The antibacterial effects of silver-based nanomaterials can be attributed to various actions, including disturbing the permeability of the cell membrane upon attachment to the bacterial wall, binding with sulfhydryl proteins to deactivate them, disrupting the respiratory chain to induce oxidative stress, and interfering with DNA replication, leading to damage to lipids[63–65]. Consequently, the bacterial wall becomes damaged, releasing the contents of the bacterial cytoplasm. All these phenomena can result in the destruction or even death of microorganisms[32,66–68] as shown in **Figure 1—6**

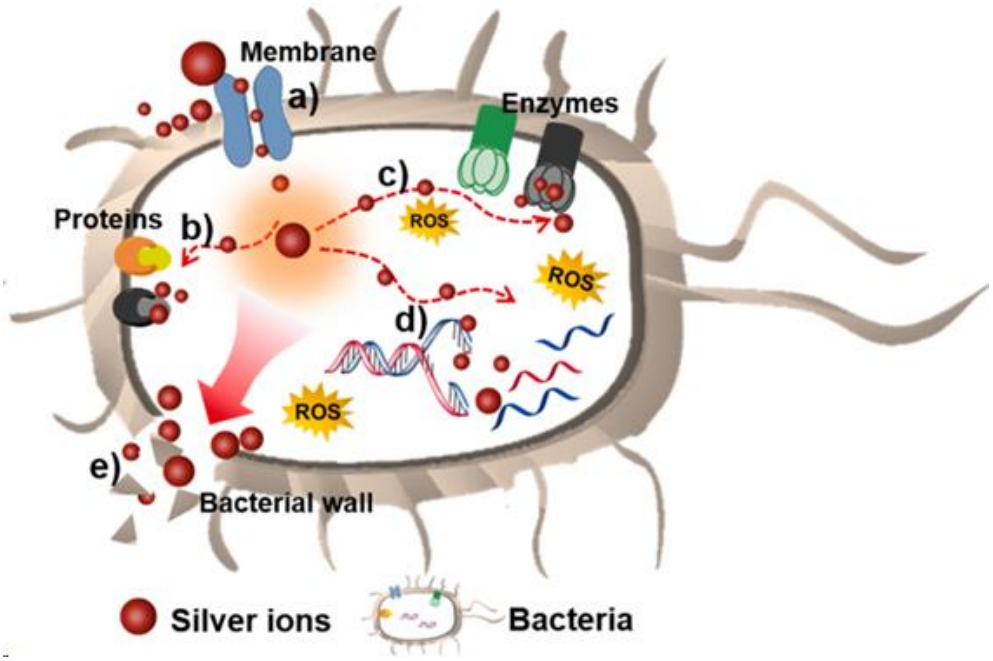

***Figure 1—6*:** Schematic illustration of antibacterial mechanisms of silver ions. Silver ions are first combined and deposited on the surfaces of bacteria and then (a) penetrate the bacterial wall and membrane. The normal metabolism of bacteria was disturbed through a series of actions such as (b) dephosphorylating the protein, (c) destroying the respiratory chain, and (d) binding to bases to make DNA lose its replication ability. Eventually, (e) the bacterial wall and membrane were broken to result in cytoplasm leaking. Reprinted with permission from reference. [69] Copyright 2021 ACS-Appl Bio Mater

1.10 Molybdenum antibacterial wound dressing

Numerous nanomaterials have been studied as potential antibacterial agents, including titanium dioxide, zinc oxide, copper oxide, silver and gold nanoparticles, molybdenum, and tungsten oxides, among others[69–71]. These nanostructured inorganic materials must adhere to specific criteria regarding their shape, size, and surface charge, as well as their chemical and physical properties to exhibit antibacterial properties[31,72–74].

The uptake of nanoparticles (NPs) by cells and their distribution primarily depends on the physicochemical characteristics of the particles. Molybdenum, as an element, doesn't possess inherent antimicrobial properties. It is an essential trace element of great significance to humans, serving as a cofactor for various enzymes like aldehyde, xanthine, and sulphite oxidase. However, molybdenum trioxide (MoO_3) has emerged as a highly promising antibacterial nanomaterial[75–80]. The antimicrobial mechanism of MoO_3 in the presence of water is explained through a dissolving process, where an acidic reaction occurs, leading to the formation of hydronium (H_3O^+) and molybdate (MoO_4^{2-}) ions. The penetration of (H_3O^+) ions through the bacterial cell wall disrupts the pH balance as well as the cell's enzyme and transport systems[81–84]. The creation of an acidic, low-pH environment due to MoO_3 nanoparticle dissolution has been reported as a universal antimicrobial agent effective against both susceptible and resistant bacterial species responsible for hospital-acquired infections[85]. The incorporation of MoO_3 into polymer coatings allows for controlled solubility and long-term use of such coatings[72,86–89].

1.11 Objective of this thesis

The goal of this thesis is to develop a cutting-edge wound dressing material that effectively combats bacterial resistance while prioritizing the safety of human cells and the environment. Our primary aim is to create a wound dressing that carefully releases silver ions in a controlled manner, with the intention of boosting its ability to fight off common wound-related pathogens *E. coli* and *B. subtilis* while maintaining its compatibility and sustainability. Ultimately, this research seeks to contribute to the advancement of wound care technology by offering the green synthesis of new composite material, that combats bacterial resistance while enhancing the antibacterial activity with fast reduction of silver ions onto the composite material and overcoming the excessive release into the environment.

The objective of Chapter 2 is to find the best-reducing agent for the reduction of silver ions onto the polyacrylonitrile (PAN) nanofiber. Enhancing antibacterial activity and suppression of tensile stress with the incorporation of molybdenum oxide nanoparticles.

The objective of Chapter 3 is the development of hybrid composite membranes with green synthesis and fast reduction of silver ions onto the membrane. Therefore, the MoO_3/PAN composite membrane was synthesized by electrospinning. In addition, the fast reduction of silver ions onto the composite membrane was studied.

References

1 J. Xue, T. Wu, Y. Dai, Y. Xia, *Chem. Rev.* **2019**, *119*, 5298.

2 B. Ding, M. Wang, X. Wang, J. Yu, G. Sun, *Mater. Today* **2010**, *13*, 16.

3 N. Bhardwaj, S. C. Kundu, *Biotechnol. Adv.* **2010**, *28*, 325.

4 S. Agarwal, J. H. Wendorff, A. Greiner, *Polymer (Guildf).* **2008**, *49*, 5603.

5 A. Keirouz, Z. Wang, V. S. Reddy, Z. K. Nagy, P. Vass, M. Buzgo, S. Ramakrishna, N. Radacsi, *Adv. Mater. Technol.* **2023**, *8*, 1.

6 N. Tucker, J. J. Stanger, M. P. Staiger, H. Razzaq, K. Hofman, *J. Eng. Fiber. Fabr.* **2012**, *7*, 63.

7 K. C. Vig Atul A.; Tripathi, Shweta; Dixit, Saurabh; Sahu, Rajnish; Pillai, Shreekumar R.; Dennis, Vida A.; Singh, Shree R., *Int. J. Mol. Sci.* **2017**, *18*, 789.

8 G. C. Han Roger I., *Adv. Ther.* **2017**, *34*, 599.

9 M. Greener, *Br. J. Sch. Nurs.* **2014**, *9*, 68.

10 O. A. Sarheed Asif; Shouqair, Douha; Boateng, Joshua S., in *Wound Healing - New insights into Ancient Challenges*, **2016**, Vol. NA, p. NA-NA.

11 W. L. B. de Carvalho Bernardo Marcelo Fabiano Gomes; Tonon, Caroline Coradi; da Silva, Jeferson Júnior; Cruz, Fernando Moraes; Martins, Adriano Luis; Höfling, José Francisco; Spolidorio, Denise Madalena Palomari, *Arch. Oral Biol.* **2021**, *125*, 105101.

12 S. E. L. . T. Bulman Giuseppe; Goswami, Parikshit; Carr, Chris; Russell, Stephen J., *Mater. (Basel, Switzerland)* **2017**, *10*, 954.

13 T. B. Velnar T; Smrkolj, Vladimir, *J. Int. Med. Res.* **2009**, *37*, 1528.

14 S. C. . P. Davis Robert, *Clin. Dermatol.* **2009**, *27*, 502.

15 D. L. . E. Church Sameer; Reid, Owen; Winston, Brent W.; Lindsay, Robert,

Clin. Microbiol. Rev. **2006**, *19*, 403.

16 S. J. Naahidi Mousa; Edalat, Faramarz; Raymond, Kevin; Khademhosseini, Ali; Chen, Pu, *J. Control. Release* **2012**, *166*, 182.

17 A. F. . W. Cardona Samuel E., *Clin. Infect. Dis.* **2015**, *61*, S69.

18 T. J. P. Cahill Bernard D, *Lancet (London, England)* **2015**, *387*, 882.

19 D. K. Sundaramurthi Uma Maheswari; Sethuraman, Swaminathan, *Polym. Rev.* **2014**, *54*, 348.

20 A. A. . V. Chaudhari Komal; Baganizi, Dieudonné R.; Sahu, Rajnish; Dixit, Saurabh; Dennis, Vida A.; Singh, Shree R.; Pillai, Shreekumar R., *Int. J. Mol. Sci.* **2016**, *17*, 1974.

21 A. R. B. Unnithan Nasser A.M.; Pichiah, P.B. Tirupathi; Gnanasekaran, Gopalsamy; Nirmala, R.; Cha, Youn-Soo; Jung, Che-Hun; El-Newehy, Mohamed H.; Kim, Hak Yong, *Carbohydr. Polym.* **2012**, *90*, 1786.

22 D. Simões, S. P. Miguel, M. P. Ribeiro, P. Coutinho, A. G. Mendonça, I. J. Correia, *Eur. J. Pharm. Biopharm.* **2018**, *127*, 130.

23 W. W. Shao Jimin; Wang, Shuxia; Huang, Min; Liu, Xiufeng; Zhang, Rui, *Carbohydr. Polym.* **2016**, *157*, 1963.

24 D. Leaper, *Int. Wound J.* **2006**, *3*, 282.

25 M. S. Mohseni Amir; Aghababaei, Zahra; Vossoughi, Manouchehr; Moravvej, Hamideh, *Artif. Organs* **2016**, *40*, 765.

26 S. D. Guo Luisa A., *J. Dent. Res.* **2010**, *89*, 219.

27 J. Salvo, C. Sandoval, *Burn. Trauma* **2022**, *10*.

28 A. Ullah, S. Ullah, M. Q. Khan, M. Hashmi, P. D. Nam, Y. Kato, Y. Tamada, I. S. Kim, *Int. J. Biol. Macromol.* **2020**, *155*, 479.

29 I. R. Liakos Loris; Scurr, David J.; Pompa, Pier Paolo; Bayer, Ilker S.; Athanassiou, Athanassia, *Int. J. Pharm.* **2013**, *463*, 137.

30 K. McElvain, J. Klister, A. Ebben, S. Gopalakrishnan, M. Dabagh, *Biomedicines* **2022**, *10*.

31 M. Farooq, M. Khalid, Y. Yoshinori, F. Wang, M. A. Iqbal, M. N. Sarwar, G. Mayakrishnan, I. S. Kim, **2023**.

32 Z. Xu, C. Zhang, X. Wang, D. Liu, *ACS Appl. Bio Mater* **2021**, *4*, 3985.

33 B. S. . B. Anisha Raja; Chennazhi, Krishna Prasad; Jayakumar, Rangasamy, *Int. J. Biol. Macromol.* **2013**, *62*, 310.

34 M. E. A. de Kraker, A. J. Stewardson, S. Harbarth, *PLoS Med.* **2016**, *13*, 1.

35 J. P. Ruparelia, A. K. Chatterjee, S. P. Duttagupta, S. Mukherji, *Acta Biomater.* **2008**, *4*, 707.

36 G. Félix, C. A. Soto-Robles, E. Nava, E. Lugo-Medina, *Chem. Res. Toxicol.* **2021**, *34*, 1970.

37 Z. Zhou, B. Li, X. Liu, Z. Li, S. Zhu, Y. Liang, Z. Cui, S. Wu, *ACS Appl. Bio Mater.* **2021**, *4*, 3909.

38 B. N. . J. Green Claire; Egan, Jonathon Todd; Rosenthal, Michael D.; Griffith, Erin A.; Evans, Marion Willard, *J. Chiropr. Med.* **2012**, *11*, 64.

39 I. S. Eleftheriadou Afroditi; Skoura, Lemonia; Dendrinou-Samara, Aikaterini; Arsenakis, Minas; Protonotariou, Efthymia; Giannousi, K., *ACS Appl. Nano Mater.* **2021**, *4*, 9799.

40 G. R. . S. Rudramurthy Mallappa Kumara; Sinniah, Uma Rani; Ghasemzadeh, Ali, *Molecules* **2016**, *21*, 836.

41 R. S. Singh M. S.; Singh, Surinder P., *J. Nanosci. Nanotechnol.* **2014**, *14*, 4745.

42 Z. Y. Yanming Xu; Xue, Jingzhe; Guo, Lu-Yin; Fang, Wei-Wei; Sun, Tian-Ci; Li, Min; Zha, Zhengbao; Yu, Qilin; Wang, Yongzhong; Zhang, Min; Lu, Yang; Cao, Baoqiang; He, Tao, *ACS Appl. Mater. Interfaces* **2020**, *12*, 4333.

43 D. Sanglard, *Front. Med.* **2016**, *3*, 11.

44 X. Ding, Q. Tang, Z. Xu, Y. Xu, H. Zhang, D. Zheng, S. Wang, Q. Tan, J. Maitz, P. K. Maitz, S. Yin, Y. Wang, J. Chen, *Burn. Trauma* **2022**, *10*.

45 L. Canchy, D. Kerob, A. Demessant, J. M. Amici, *J. Eur. Acad. Dermatology Venereol.* **2023**, *37*, 7.

46 C. Hwang, M. H. Choi, H. E. Kim, S. H. Jeong, J. U. Park, *NPG Asia Mater.* **2022**, *14*.

47 R. D. Laxminarayan Adriano; Wattal, Chand; Zaidi, Anita K. M.; Wertheim, Heiman F. L.; Sumpradit, Nithima; Vlieghe, Erika; Hara, Gabriel Levy; Gould, Ian M.; Goossens, Herman; Greko, Christina; So, Anthony D.; Bigdeli, Maryam; Tomson, Goeran; Woodhouse, Will;, *Lancet. Infect. Dis.* **2013**, *13*, 1057.

48 K. J. Woo, C. K. Hye, W. K. Ki, S. Shin, H. K. So, H. P. Yong, *Appl. Environ. Microbiol.* **2008**, *74*, 2171.

49 B. B. Boonkaew Philip Martin; Rengpipat, Sirirat; Supaphol, Pitt; Kempf, Margit; He, Jibao; John, Vijay T.; Cuttle, Leila, *J. Pharm. Sci.* **2014**, *103*, 3244.

50 J. R. E. Morones Jose Luis; Camacho, A.; Holt, Katherine B.; Kouri, Juan B.; Ramirez, Jose Tapia; Yacaman, Miguel Jose, *Nanotechnology* **2005**, *16*, 2346.

51 S. S. Thammawithan Pawinee; Nasompag, Sawinee; Daduang, Sakda; Klaynongsruang, Sompong; Prapasarakul, Nuvee; Patramanon, Rina, *Vet. Sci.* **2021**, *8*, 177.

52 A. Rana, S. Pathak, D. K. Lim, S. K. Kim, R. Srivastava, S. N. Sharma, R.

Verma, *ACS Appl. Nano Mater.* **2023**, *6*, 8106.

53 Y. Meng, L. Chen, Y. Chen, J. Shi, Z. Zhang, Y. Wang, F. Wu, X. Jiang, W. Yang, L. Zhang, C. Wang, X. Meng, Y. Wu, W. Bu, *Nat. Commun.* **2022**, *13*, 1.

54 M. Vincent, R. E. Duval, P. Hartemann, M. Engels-Deutsch, *J. Appl. Microbiol.* **2018**, *124*, 1032.

55 B. E. Kim, T. Nevitt, D. J. Thiele, *Nat. Chem. Biol.* **2008**, *4*, 176.

56 H. Yuan, L. Chen, F. F. Hong, *ACS Appl. Mater. Interfaces* **2020**, *12*, 3382.

57 A. Frei, A. D. Verderosa, A. G. Elliott, J. Zuegg, M. A. T. Blaskovich, *Nat. Rev. Chem.* **2023**, *7*, 202.

58 L. Wang, C. Hu, L. Shao, *Int. J. Nanomedicine* **2017**, *12*, 1227.

59 M. L. Ermini, V. Voliani, *ACS Nano* **2021**, *15*, 6008.

60 A. P. Kornblatt, V. G. Nicoletti, A. Travaglia, *J. Inorg. Biochem.* **2016**, *161*, 1.

61 L. García-Cruz, V. Montiel, J. Solla-Gullón, *Shape-controlled metal nanoparticles for electrocatalytic applications*, De Gruyter, **2019**.

62 D. McShan, P. C. Ray, H. Yu, *J. Food Drug Anal.* **2014**, *22*, 116.

63 H. S. Abdo, K. A. Khalil, S. S. Al-Deyab, H. Altaleb, E. S. M. Sherif, *Fibers Polym.* **2013**, *14*, 1985.

64 A. Mahapatra, N. Garg, B. P. Nayak, B. G. Mishra, G. Hota, *J. Appl. Polym. Sci.* **2012**, *124*, 1178.

65 V. Kostenko, J. Lyczak, K. Turner, R. J. Martinuzzi, *Antimicrob. Agents Chemother.* **2010**, *54*, 5120.

66 C. B. Tanase Lavinia; Coman, Năstaca Alina; Roșca, Ioana; Man, Adrian; Toma, Felicia; Mocan, Andrei; Nicolescu, Alexandru; Jakab-Farkas, László; Biro, D.; Mare, Anca, *Nanomater. (Basel, Switzerland)* **2019**, *9*, 1541.

67 C. A. S. . B. Ballesteros Juliana Cancino; Correa, Daniel S.; Zucolotto, Valtencir, *ACS Appl. bio Mater.* **2019**, *2*, 644.

68 H. Lv, S. Cui, Q. Yang, X. Song, D. Wang, J. Hu, Y. Zhou, Y. Liu, *Mater. Sci. Eng. C* **2021**, *118*, 111331.

69 Z. Xu, C. Zhang, X. Wang, D. Liu, *ACS Appl. Bio Mater.* **2021**, *4*, 3985.

70 S. Zhang, Y. Tang, B. Vlahovic, *Nanoscale Res. Lett.* **2016**, *11*, 1.

71 M. R. Mulenos, J. Liu, H. Lujan, B. Guo, E. Lichtfouse, V. K. Sharma, C. M. Sayes, *Environ. Chem. Lett.* **2020**, *18*, 1319.

72 C. Zollfrank, K. Gutbrod, P. Wechsler, J. P. Guggenbichler, *Mater. Sci. Eng. C* **2012**, *32*, 47.

73 S. Kothaplamoottil Sivan, A. K. K. Padinjareveetil, V. V. T. Padil, R. Pilankatta, B. George, C. Senan, M. Černík, R. S. Varma, *Clean Technol. Environ. Policy* **2019**, *21*, 1549.

74 S. Jadhav, S. Gaikwad, M. Nimse, A. Rajbhoj, *J. Clust. Sci.* **2011**, *22*, 121.

75 A. Jayakumar, S. Mathew, S. Radoor, J. T. Kim, J. W. Rhim, S. Siengchin, *Mater. Today Chem.* **2023**, *30*, 101492.

76 W. Cao, L. Yue, Z. Wang, *Carbohydr. Polym.* **2019**, *215*, 226.

77 J. Liao, L. Wang, S. Ding, G. Tian, H. Hu, Q. Wang, W. Yin, *Nano Today* **2023**, *50*, 101875.

78 T. I. Kim, B. Kwon, J. Yoon, I. J. Park, G. S. Bang, Y. K. Park, Y. S. Seo, S. Y. Choi, *ACS Appl. Mater. Interfaces* **2017**, *9*, 7908.

79 Y. Yang, M. Li, C. Zhou, K. Zhou, J. Yu, Y. Su, N. Hu, Y. Zhang, *Langmuir* **2021**, *37*, 1596.

80 Y. Zhong, X. T. Zheng, S. Zhao, X. Su, X. J. Loh, *ACS Nano* **2022**, *16*, 19840.

81 M. Zhu, X. Liu, L. Tan, Z. Cui, Y. Liang, Z. Li, K. W. Kwok Yeung, S. Wu, *J. Hazard. Mater.* **2020**, *383*, 121122.

82 U. Gradišar Centa, P. Kocbek, A. Belcarz, S. D. Škapin, M. Remškar, *J. Nanomater.* **2020**, *2020*.

83 C. Zollfrank, K. Gutbrod, P. Wechsler, J. P. Guggenbichler, *Mater* **2012**, *32*, 47.

84 I. Shakir, M. Shahid, D. J. Kang, *Chem. Commun.* **2010**, *46*, 4324.

85 T. L. Wang Xiangmei; Zhu, Yizhou; Cui, Zhenduo; Yang, Xianjin; Pan, Haobo; Yeung, Kelvin W.K.; Wu, Shuilin, *ACS Biomater. Sci. Eng.* **2017**, *3*, 816.

86 C. Zollfrank, K. Gutbrod, P. Wechsler, J. P. Guggenbichler, *Mater. Sci. Eng. C* **2012**, *32*, 47.

87 Catherine E. Housecroft and Alan G. Sharpe, *The alkali metals*, **1935**.

88 D. Hyeon Shin, S. Hwang, Y. Seo Park, J. Kim, S. Lee, S. Hong, S. Eun Shim, Y. Qian, *Appl. Surf. Sci.* **2022**, *595*, 153496.

89 A. I. Ribeiro, A. M. Dias, A. Zille, *ACS Appl. Nano Mater.* **2022**, *5*, 3030.

CHAPTER 2. Incorporation of molybdenum oxide nanoparticles into PAN nanofiber and study of different reducing agents

2.1 Introduction:

The skin, as the outermost organ of the human body, acts as the primary defense against external microorganisms[1]. When the skin is injured, it becomes susceptible to the entry of microbes into wounds or the body, which can lead to serious consequences such as persistent infection, inflammation, or even death[2]. Wound dressing plays a crucial role in managing and promoting the healing of various types of wounds. It involves applying materials or products to cover and protect the injured area, creating an optimal environment for natural healing. Wound dressings have multiple functions, including providing a barrier against external contaminants, controlling moisture levels, promoting tissue regeneration, and reducing the risk of bacterial infection[3,4]. Advances in wound dressing technology have resulted in different types of dressings, such as gauze dressings, hydrogels, foams, films, and specialized antimicrobial dressings that contain substances like nanoparticles[5–7], antibiotics [8], and plant extracts[9,10]

The utilization of silver nanoparticles (AgNPs) in wound dressings has emerged as a promising strategy in the field of wound care and management. AgNPs have inherent antimicrobial properties that effectively combat multiple microorganisms, including bacteria, fungi, and viruses[11]. The surface area of nanoparticles is so high, which enhances their antimicrobial efficacy. When integrated into wound dressings, AgNPs enable the sustained release of silver ions, creating an environment that inhibits bacterial growth and fosters wound healing. Moreover, AgNPs have been studied to induce the release of reactive oxygen species (ROS), generating potent bactericidal free-radicals[12]. The synthesis of AgNPs commonly involves reducing agents, sodium hydroxide[13–15] (NaOH), sodium borohydride[16–18] ($NaBH_4$), sodium citrate[19–22], and UV irradiation[23]. Each reducing agent possesses unique properties that can influence the

characteristics of the resulting AgNPs and their release within wound dressings. Therefore, a comparative study of these reducing agents is crucial for understanding their advantages, limitations, and suitability for wound dressing applications.

Polyacrylonitrile (PAN) nanofibers are inherently delicate and lack sufficient mechanical strength for practical use. However, the incorporation of molybdenum trioxide (MoO_3) nanoparticles into PAN nanofibers can enhance their mechanical properties[24,25].Molybdenum oxide (MoO_3) functions as a reinforcement agent[25], augmenting the tensile strength and stability of the nanofiber matrix[26]. This improved mechanical strength is vital for the durability and longevity of wound dressings, ensuring their effective implementation in clinical settings. By integrating MoO_3 into PAN nanofibers, the resulting composite material can provide an additional antimicrobial effect[27], contributing to the prevention and control of infections during the wound healing process[28]. In recent years, electrospinning has emerged as a pivotal technique for fabricating functional nanomaterials, positioning itself as a versatile method for various advancements. Notably, electrospinning, essentially a physical drying process[29], has extended its capabilities in multiple directions. These extensions include the creation of core-shell structures[30], Janus configurations[31], and hybrid architectures through the utilization of multi-fluid processes. The ability to scale up nanofiber production has also marked a significant stride. Additionally, electrospun nanofibers can be tailored extensively through subsequent treatments to fine-tune their functional attributes. The ease with which these treatments can be applied contributes to the versatility of electrospinning in enhancing nanofiber functionality.The controlled release of silver from wound dressings plays a vital role in their antimicrobial efficacy and wound healing properties. Silver-based wound care products can impede bacterial

growth; however, excessive silver release can lead to toxicity in wounds[32,33]. Sustained release of silver, whether at a high or low concentration, is crucial for effective wound dressing. In the absence of sustained silver release, bacterial recolonization of the wound may occur[34]. The choice of reducing agents significantly influences the quantity of silver ions released and the rate of release, which, in turn, impacts the antimicrobial effect. Hence, selecting the appropriate reducing agents to produce silver nanoparticles (AgNPs) is essential to achieve an optimal release profile for the desired antimicrobial effect within the infected wound.

In this study, the authors examined the release profile of silver (Ag) and its antibacterial activity using different reducing agents on MoO_3/PAN nanofiber film. They conducted a detailed analysis of the physical and chemical structure of Ag-MoO_3/PAN nanofiber mats, providing valuable insights into their composition and properties. These findings contribute to our understanding of their potential applications in wound dressing and antimicrobial therapy. Additionally, this study aims to determine the most effective reducing agent for doping of Ag nanoparticles on the surface of nanofiber membranes (NFMs). By comparing the Ag^+ ions release profile and antibacterial activity achieved with different reducing agents on the MoO_3/PAN nanofiber film also discuss.

2.2 Experimental methods

2.2.1 Preparation of MoO_3/PAN nanofiber membrane

Molybdenum oxide (MoO_3), sodium citrate dihydrate (≥ 99 \%), sodium borohydride ($NaBH_4$), and PAN (Mw 150,000 g/mol) was purchased from Sigma-Aldrich, Tokyo, Japan. N, N- Dimethylformamide (DMF, 99.8%), silver nitrate (AgNO3, 99.8%), and sodium hydroxide (NaOH, 97.0%), were purchased from FUJIFILM Wako Pure Chemical Ltd, Japan. Escherichia coli (Hrf 3000) was provided from the Coli Genetic Stock (CGSC; Yale University, New Haven, CT, USA). Bacillus subtilis (168) was provided from Dr. Ogasawara, Shinshu University, Japan. Luria–Bertani broth was supplied in an analytical grade from Nacalai Tesque, Inc., Kyoto, Japan. The Petri dishes were purchased from Sansei Medical Co., Ltd., Japan. Milli-Q water (Direct-Q UV3) was used in the experiments.

2.2.2 Compositional analysis

Field emission scanning electron microscopy (FE-SEM, JSM-IT800SHL, Japan), and high-resolution transmission electron microscope (TEM, JEOL, JEOL2010, Japan, 200kV accelerating voltage) were used to record the morphology and elemental composition of the membrane. Crystal structuring was characterized by X-ray diffraction (XRD, Rigaku, MiniFlex300, Japan with monochromatic CuKα radiation at 33 kV). The Fourier transform infrared (FT/IR-6600) and X-ray photoelectron spectroscopy (XPS, AXIS-ULTRA HSA SV, Japan) were performed to thoroughly characterize the chemical structure and morphology of NFMs. FTIR analysis, 72 scans at a resolution of 4 cm−1 were performed for each sample all spectra presented in the wave number range 400–4000 cm−1. Contact angle measurement was analyzed by Hololab 5000, Japan with de-ionized water. Thermogravimetric analysis (Thermo plus

TG-8120, Japan) of polymers was measured as weight change analysis. Silver release content was measured by Inductively coupled plasma optical emission spectrometry (ICP-OES, SPS 5000, HORIBA, Japan). UV lamp light (WFH-204B, Shanghai Int. USA) was used as a reducing agent.

2.2.3 Membrane fabrication

For the preparation of MoO_3/PAN. In a typical synthesis, a 10% PAN was dissolved in 10 cm^3 DMF to form a transparent solution. 1% molybdenum oxide nanoparticles w.r.t polymer was added into a 10% polymer solution to form a viscous solution. After complete dispersion, the solution was loaded into the 10 mL plastic syringe equipped with a needle of 0.8 mm diameter. The flow rate of the syringe pump was 1.0 mL h^{-1} and the distance between the collector and the needle was 18.0 cm. The applied voltage was held at 15 kV. The humidity was kept at 40 ± 5 %. Electrospun fibrous membranes were ripped down from the sheet pan and vacuum dried at 70 °C for 24 h to remove the DMF and other volatile residuals. As-obtained NFMs were ready for further characterization.

2.2.4 Synthesis of Ag-MoO_3/PAN nanofibers

Four Petri dishes containing 50 ml $AgNO_3$ solutions were prepared with 0.1M concentration. The approximately 50 mg MoO_3/PAN nanofiber sheets were simultaneously submerged into the Petri dishes. Afterward, these dishes were sealed to avoid changing concentrations due to vaporization. All dishes were vigorously shaken at 300 rpm (Rotary shaker NA-301 N, Nissin, Japan) for 6 h. After the required time one sample dish was placed under UV light again for 6 h (254 nm, 100 V, 60 Hz, 0.7 A, XX-15NF/J, Spectroline, USA) to facilitate the formation of AgNPs on the surfaces of MoO_3/PAN nanofiber. While three samples were removed from the $AgNO_3$ solution and

added into 0.1 M reducing agent solutions (NaOH, $NaBH_4$, and Sodium citrate) for 3 h to reduce the Ag^+ ions to AgNPs. Next, all the samples were collected and thoroughly washed with distilled water (DW) multiple times. Subsequently, the samples were dried for 24 hours at 60°C using a program-controlled oven (AS ONE DOV-600P, MonotaRo Co., Ltd., Japan) before proceeding with further tests. These processed samples were designated as A (NaOH), B ($NaBH_4$), C (sodium citrate), and D (UV only) reduced nanofibers.As described in **Figure *2—1***

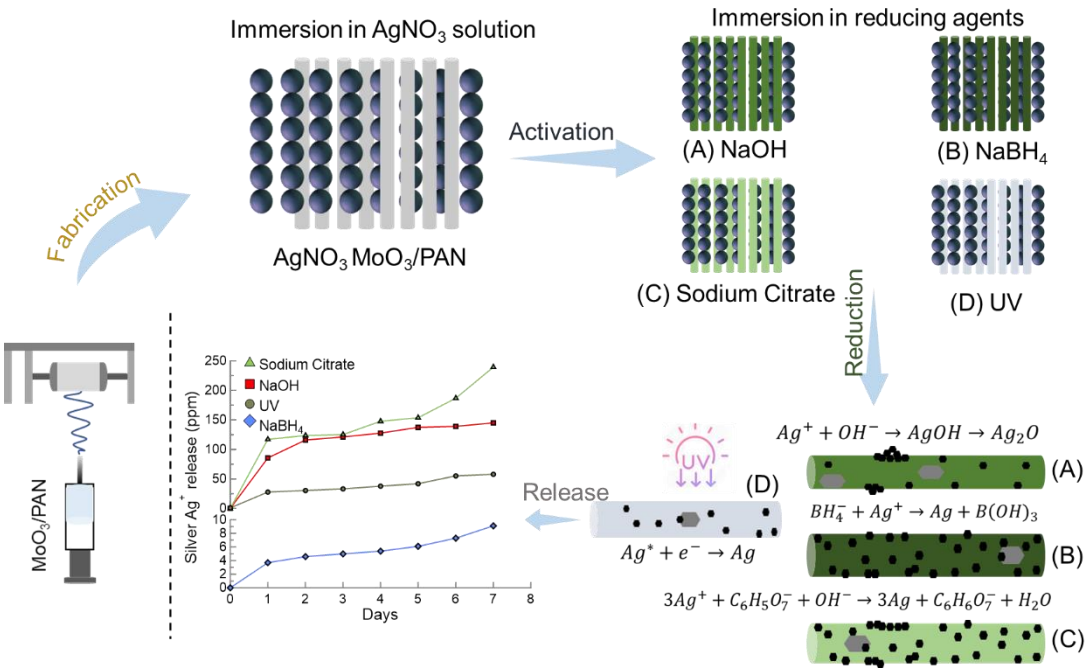

Figure 2—1: Schematic representation of silver nanoparticle doping onto the surface of the MoO_3/PAN nanofiber membrane treated with different reducing agents (A) NaOH, (B) $NaBH_4$, (C) and sodium citrate and (D) under UV and the silver release profile.

2.3 Results and discussions

The Ag-MoO_3/PAN nanofiber membranes with different reducing agents are demonstrated in **Figure *2—2***. The synthesis of Ag-MoO_3/PAN NFMs followed previous reports with details in the experimental section of supplementary material. The

crystallite structure of MoO_3/PAN was analyzed by X-ray diffraction (XRD). As shown in Figure 2—2, all the characteristic peaks observed at 12.76°, 23.32°, 25.70°, 27.33° and 29.69° 34.36° 38.97° 46.28° 49.23°correspond to (020), (110), (040), (021), (130) (140), (060), (210), (002) respectively, that are planes of monoclinic MoO_3 (JCPDS No. 000-05-0508). Furthermore, no peaks were observed confirming no other impurities and good crystallinity of MoO_3 in PAN nanofiber. Typically PAN peak was observed near 17. 50°.The molybdenum oxide content is 0.1% w.r.t 10% PAN in the NFMs with amorphous structure.

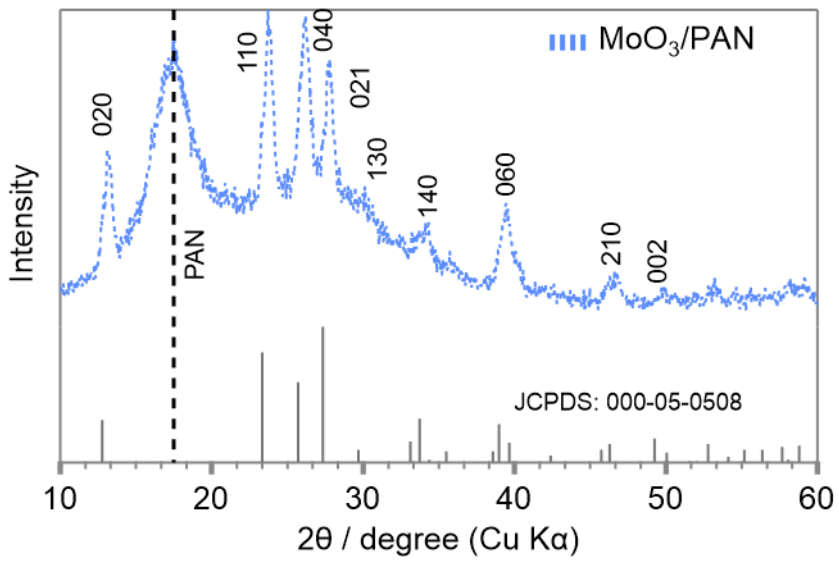

Figure 2—2:XRD pattern of MoO_3/PAN and their reference JCPDS number.

2.4 X-ray Diffraction

The as-prepared MoO_3/PAN nanofiber membranes (NFMs) were subjected to reduction by immersion in a 0.1 M $AgNO_3$ solution using various reducing agents (i.e : NaOH, $NaBH_4$, sodium citrate, and UV light). The X-ray diffraction (XRD) pattern with different reducing agents of Ag-MoO_3/PAN NFMs displayed in **Figure *2—3***, along with the mapping images presented in **Figure *2—4***, simultaneously validate the presence of

AgNPs loaded onto the surface of the reduced NFMs. The growth of silver nanoparticles (AgNPs) on the surface of the NFMs was observed, as evidenced by the transmission electron microscopy (TEM) and field emission scanning electron microscopy (FE-SEM) images provided in **Figure *2—4***.

2.4.1 Sodium hydroxide (NaOH).

The X-ray diffraction (XRD) pattern of the Ag-MoO_3/PAN nanofiber film is presented in **Figure *2—3***A. The XRD analysis reveals the crystalline nature of the synthesized silver nanoparticles (AgNPs), as evidenced by the presence of distinct peaks at 26.67°, 32.81°, 38.01°, 54.95°, 65.5°, and 68.8°. These peaks correspond to the crystallographic planes of silver oxide Ag_2O (JCPDS No.000-041-1104), specifically the 110, 111, 200, 220, 311, and 222 planes, respectively.

2.4.2 Sodium borohydride ($NaBH_4$).

The XRD analysis of **Figure *2—3***B reveals the crystalline nature of the synthesized silver nanoparticles (AgNPs), as evidenced by the presence of distinct peaks at 38.78°, 44.13°, 64.67°, and 78.29°. These peaks correspond to the crystallographic planes of the silver nanoparticles, specifically the 111, 200, 220, and 311 planes, respectively. These findings agree with the silver nanoparticles identified in the (JCPDS No.000-003-0931)

2.4.3 Sodium citrate.

The X-ray diffraction (XRD) pattern presented in **Figure *2—3***C demonstrates that sodium citrate exhibits a relatively weak reducing effect compared to NaOH and $NaBH_4$, resulting in less significant alteration of the MoO_3 crystal structure in the Ag-MoO_3/PAN nanofiber. The XRD analysis reveals weak crystalline peaks between 25.0° and 29.7°, indicating the presence of molybdenum oxide. Additionally, a strong peak is observed near 30.0° and 35.1°, corresponding to the silver nanoparticles with

crystallographic planes 200, 140, and 220, respectively. The overall XRD patterns suggest the formation of silver molybdenum oxide, specifically $Ag_2(Mo_2O_7)$ (JCPDS No.000-003-0931).

2.4.4 Ultraviolet (UV) reduction.

UV reduction has minimal impact on the crystal structure of PAN, as evidenced by the persistent strong peak near 17.50°, which corresponds to the PAN peak. In contrast, the XRD patterns obtained with other reducing agents exhibit relatively weak peaks. The XRD analysis of the synthesized MoO_3 component displays peaks at 27.04°, 31.82°, 33.28°, 38.62°, 50.88°, and 55.76°, corresponding to the crystallographic planes 311, 222, 400, 511, and 440, respectively. These findings indicate the formation of silver molybdenum oxide, specifically Ag_2MoO_4 (JCPDS No.01-083-9163), demonstrate in **Figure *2*—*3***D.

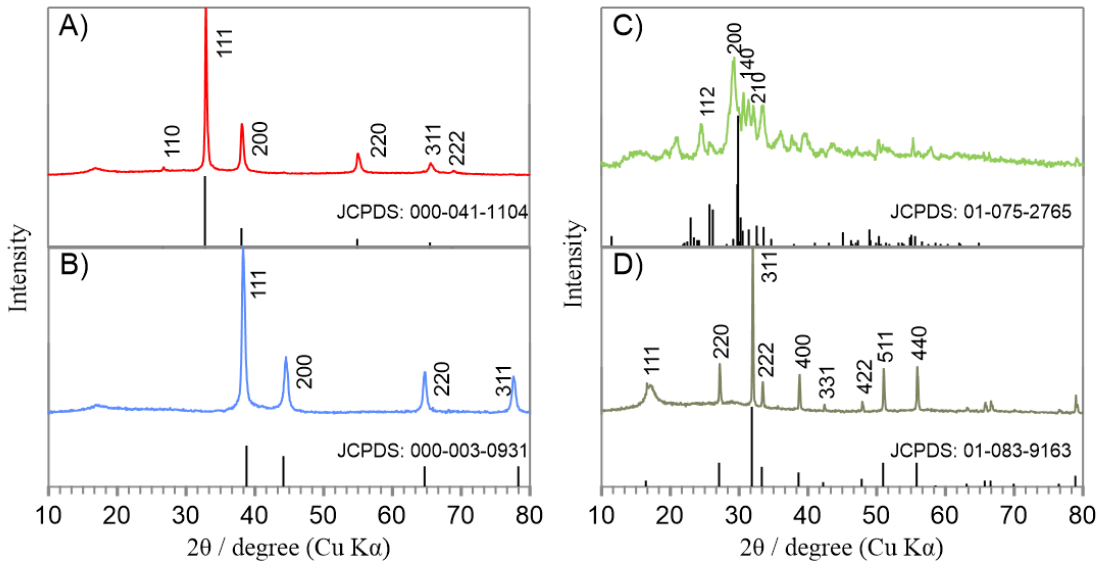

Figure 2—3: XRD pattern of Ag-MoO_3/PAN nanofiber membrane with different reducing agents A) NaOH, B) $NaBH_4$, C) sodium citrate, and D) UV only.

2.5 Compositional analysis:

Figure *2—4* illustrates the impact of reducing agents in depositing silver nanoparticles onto as-synthesized MoO_3/PAN nanofibers. The images captured through transmission electron microscopy (TEM) and scanning electron microscopy (SEM) provide valuable insights, along with corresponding elemental distribution mappings, into the resulting Ag-MoO_3/PAN nanofiber membranes. Samples reduced using $NaBH_4$ (B) and sodium citrate (C) show a uniform distribution of silver nanoparticles, clearly demonstrating their even dispersion on nanofiber. Conversely, samples reduced with NaOH (A) exhibit agglomeration of silver nanoparticles, and only a minimal number of nanoparticles were deposited on the surface and under UV (D) irradiation.

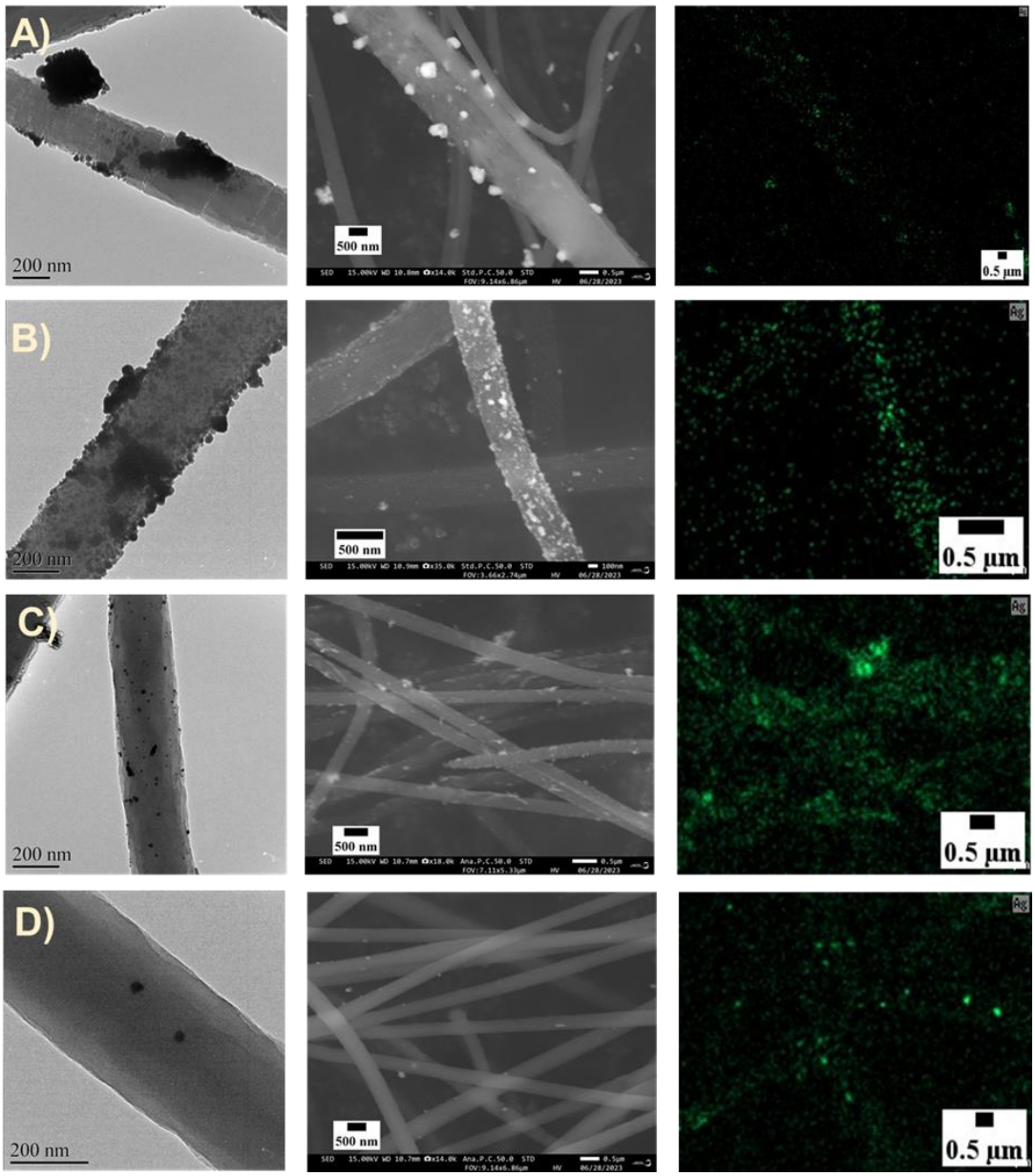

Figure 2—4: TEM, SEM, and elemental mapping of Ag-MoO_3/PAN nanofiber membrane with different treatment A) NaOH, B) $NaBH_4$, C) sodium citrate, D) UV

2.6 Fourier transform infrared (FT-IR) analysis.

FTIR measurements were performed to analyze the functional groups responsible for the reduction of Ag^+ and capping/stabilization of silver nanoparticles. By comparing the observed intense bands with standard values, the presence of specific functional

groups was identified. The FTIR spectrum exhibited absorption bands at various wavenumbers, including 3629, 2940, 2323, 2319, 2243, 1542, 1453, 1361, 1258, 801, 774, and 420 cm^{-1}, indicating the involvement of a capping agent in the nanoparticles' formation **Figure *2—5***. Furthermore, peaks at 1656 cm^{-1} and 2242 cm^{-1} indicated the presence of the cyano group (C≡N) present in PAN. This suggested that the possibility of coordination bonds forming between PAN and silver was negligible. The peaks at 1451 and 2920 cm-1 represented the bending and stretching vibrations of the $C–H_2$ functional group in PAN, respectively. The peak at 1745 cm^{-1} was attributed to C = O, resulting from PAN oxidation in air. Additionally, the peaks at 536 cm^{-1} and 1745 cm^{-1} were assigned to C = O bending and C = O stretching, respectively. Moreover, the peaks at 1250 cm^{-1} and 1357 cm^{-1} were related to CH group vibrations of CH and CH_2, respectively. Regarding molybdenum, as it is significantly heavier than oxygen, the system's vibrations mainly involved the oxygen atoms. The characteristic peaks of MoO_3 nanoparticles were observed predominantly in the range of 1000 to 400 cm^{-1} range. Notably, the peak at 801 cm^{-1} was attributed to the alternate bond length of MoO_3, while the peak at 549 cm^{-1} was related to the complexation of an oxygen atom with three different molybdenum atoms.

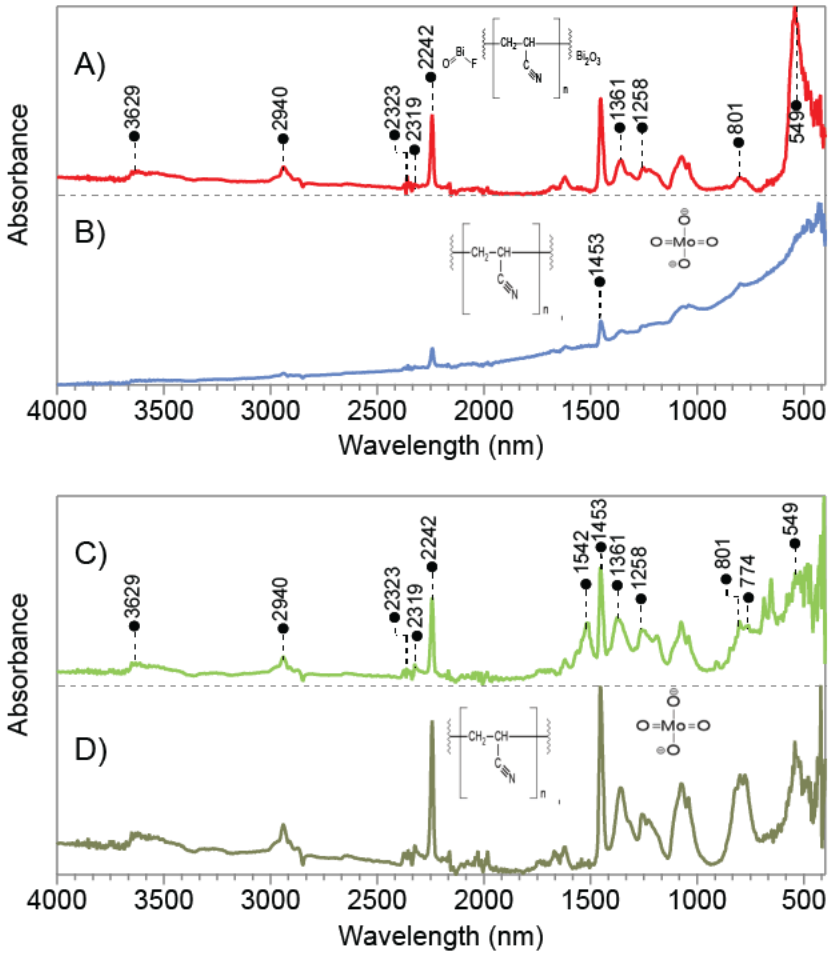

Figure 2—5: IR spectra of Ag-MoO_3/PAN nanofiber membrane with different reducing agent treatments(A) NaOH, (B) $NaBH_4$, (C) sodium citrate under UV, and (D) UV only.

2.7 X-ray photoelectron spectroscopy (XPS) analysis

The XPS study provided valuable information to determine the percentage composition of Ag, O, N, and S elements in nanofiber AgNPs. Utilizing the XPS data, we calculated the surface composition (Ci) and the percentages of Ag-O, Ag-N, and Mo-O using the following equation (1). The XPS spectrum of sample B with $NaBH_4$ reducing agent exhibits one characteristic doublet of hexavalent molybdenum at 230.0 and 234.1 eV, which correspond to Mo 3d3/2 and Mo 3d5/2 orbitals, respectively. The intensity of the Mo 3d 5/2 of sample B is lower possibly due to the strong reducing agent, and poor

electrical conductivity of the physical mixture of oxide powder into the PAN nanofiber. In all samples the strong peak of Ag 3d shows the existence of silver on MoO_3/PAN nanofiber. The wide scan XPS spectrum and relatively strong peak were shown in **Figure *2—6***

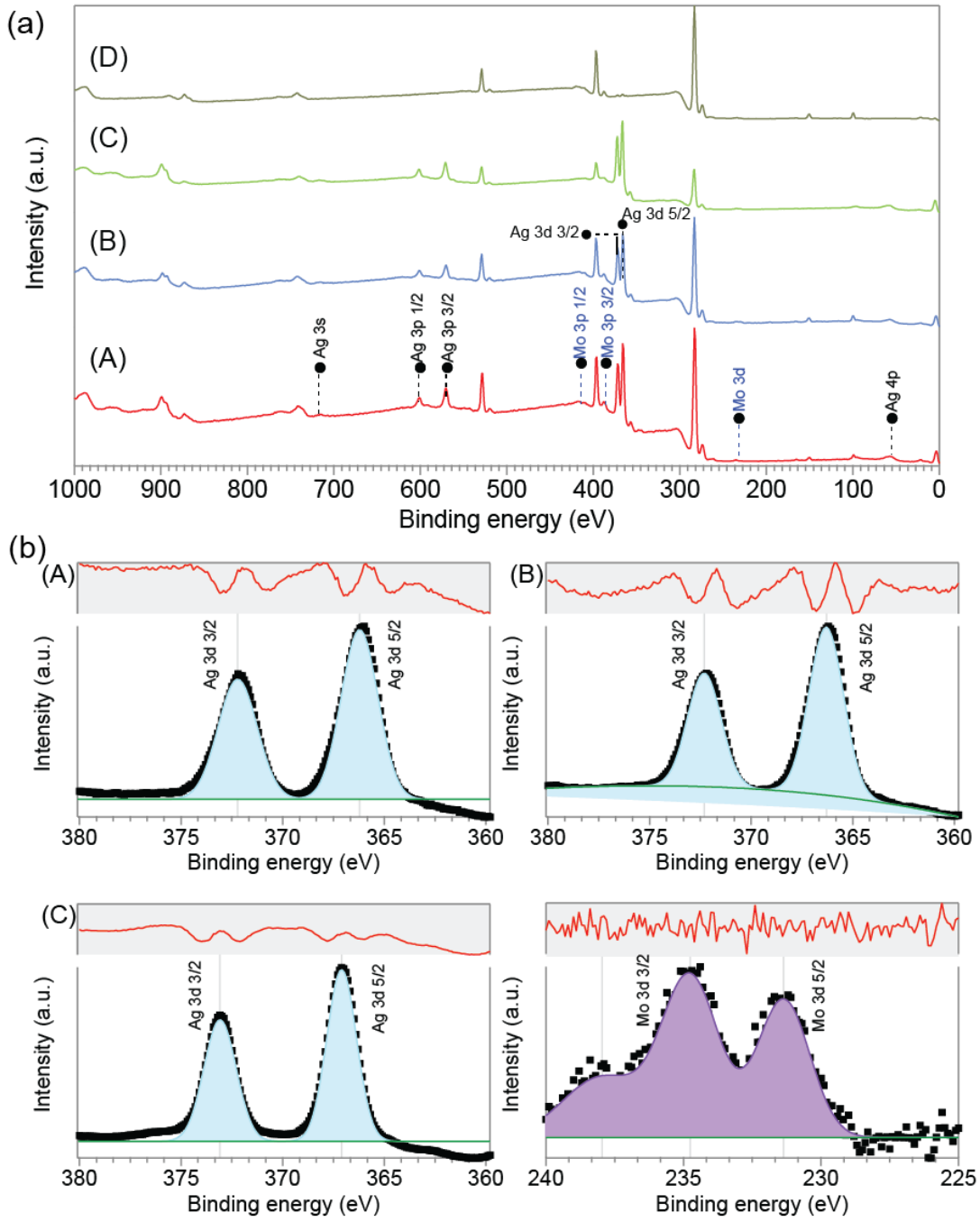

Figure 2—6: (a) The wide-scan XPS spectrum of A) NaOH, B) $NaBH_4$, C) sodium citrate, and D) UV only treated Ag-MoO_3/PAN nanofiber membrane.(b) XPS spectra of sample A) NaOH, B)$NaBH_4$, C) sodium citrate treated Ag-MoO_3/PAN nanofiber membrane of Ag-3d and sample (C) of Mo-3d,black dotted lines were observed and area under the line were gauss fitting.

2.8 Thermogravimetric analysis (TGA)

TGA was then performed on the material to find the weight percent of each material. The TGA analysis curve with sample-A NaOH treated (21.41% of the polymer), sample-B $NaBH_4$ treated (54.89% of the polymer), sample C- Sodium citrate (48.01% of the polymer) and sample- C with UV only (80% of the polymer) were shows weight loss peak at different temperatures of combustion or evaporation (**Figure *2—7*** A-D). Some unusual shapes of the curve are due to the cooling that followed the reactive overheating. Silver doped MoO_3/PAN degradation was observed at around 325℃ in all samples. The sample A treated with NaOH is seen to be more thermally stable than other reducing agents. $NaBH_4$ treated sample the degradation occurs in 4 steps. The highest weight loss in UV treated samples only as compared to other reducing agents, may be due to the absence of any other materials. TGA analysis of 10% PAN and 10% PAN/MoO_3 were represented in **Figure *2—7*** E-F.

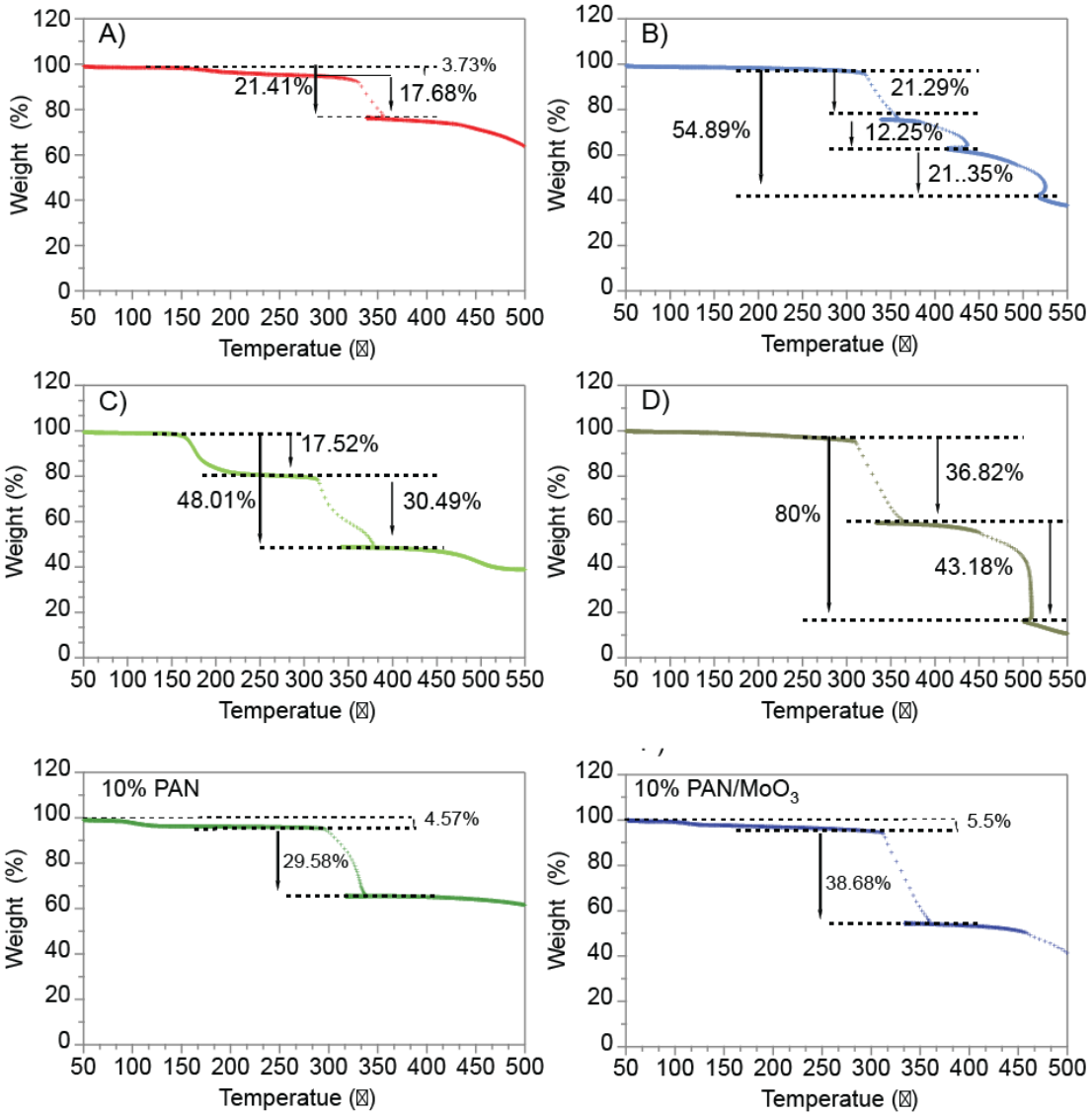

Figure 2—7: TGA analysis of Ag-MoO_3/PAN nanofiber membranes treated with different reducing agents A) NaOH, B) $NaBH_4$, C) sodium citrate, and D) UV only where E) 10%PAN,and F) MoO_3/PAN.

2.9 Water contact angle.

The water contact angle variations observed on Ag-MoO_3/PAN nanofiber shows in **Figure *2—8***, surfaces under different treatments provide valuable insights into how these surface modifications affect the wettability and hydrophilicity of the nanofibers,

consequently influencing their interaction with bodily fluids, such as wound exudate. Treatment with NaOH reducing agent resulted in a higher contact angle (105°), indicating reduced surface wetting. This hydrophobic surface property can be advantageous for wound dressing applications as it helps repel water, preventing excessive moisture buildup and potentially enhancing wound healing by reducing the risk of infection or maceration[35]. On the other hand, treatment with $NaBH_4$ resulted in a lower contact angle (56°), indicating increased surface wetting and enhanced wettability. This hydrophilic characteristic facilitates the absorption of wound exudate, promoting a moist wound healing environment. Improved hydrophilicity also aids in better fluid distribution and contact with the wound bed, potentially facilitating the delivery of therapeutic agents and creating a suitable environment for tissue regeneration processes[5]. Treatment with sodium citrate exhibited a similar effect to $NaBH_4$, further enhancing wettability (60° contact angle). Additionally, exposure to UV light resulted in a slightly lower contact angle (53°), suggesting a minor increase in surface wetting. This improved wettability can promote better fluid absorption in wound dressings and contribute to wound healing[36]. Moreover, UV light exposure has the added advantage of potential antimicrobial effects, reducing the risk of infection[37,38]. Overall, these varying contact angles highlight the ability of surface modifications to tailor the wettability and hydrophilicity of Ag-MoO_3/PAN nanofibers to meet specific requirements for wound dressing applications.

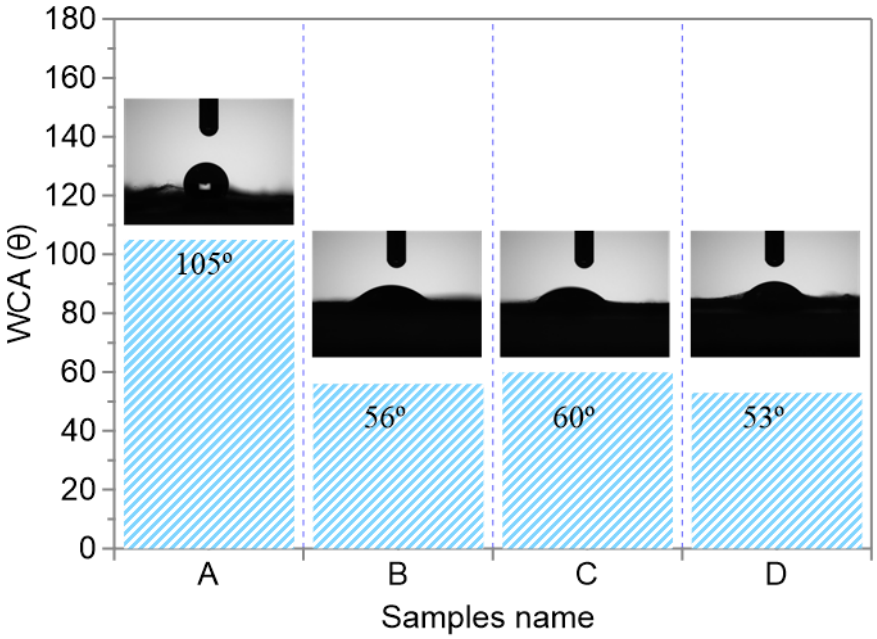

Figure 2—8: Water contact angle of Ag-MoO_3/PAN membrane under different reducing agents' treatment, A) NaOH, B) $NaBH_4$, C) sodium citrate, and D) UV

2.10 Ag^+ ions release profile.

The antibacterial activity of Ag-incorporated NFMs is closely linked to the kinetic dynamics and quantitative release of Ag^+ ions We conducted an assessment to measure the releasing rates and amounts of silver (ppm) from Ag-MoO_3/PAN with various reducing agents represented in **Figure *2—9*** a. To determine the release behavior for all Ag-MoO_3/PAN samples, we utilized inductively coupled plasma (ICP-OES) with standard solutions having silver concentration of 0.5, 1, 5, and 10 ppm were prepared for making a standard calibration curve. The coefficient factor R^2 was found to be 0.999 shown in **Figure *2—9***b. The procedure for measuring the release profile was followed by previous report[5].The silver release profiles provide insights into the sustained release of silver ions from Ag-MoO_3/PAN nanofibers over time. Silver ions are known for their antimicrobial properties. The release of silver ions from the nanofibers is influenced by the different treatments: NaOH treatment: The silver release steadily increased from

Day 0 (2 ppm) to Day 7 (144.82 ppm), indicating continuous release of silver ions. $NaBH_4$ treatment: The silver release also increased gradually from Day 0 (1.2 ppm) to Day 7 (9.1 ppm), indicating sustained release of silver ions. Sodium citrate treatment: The silver release exhibited a more significant increase, reaching 239.36 ppm by Day 7, suggesting a higher rate of silver ion release. This higher rate could be pH of the solution alter, and the chelating effect of sodium citrate that enhance their solubility and facilitating their release of silver ions from nanofiber[39]. UV exposure: The silver release showed a similar increasing trend, with the highest release observed on Day 7 (57.89 ppm).

Additionally, we fitted the release data of Ag-MoO_3/PAN samples to different models, as described in a previous report[40] The release data showed better fitting toward Peppas and first-order models, as shown in **Figure *2—9***c-d, which we surmise that more than one type of mechanism involved. Korsmeyer-Peppas model describes the release of drug in general fitting approach.

$$F = kt^n \qquad (1)$$

The drug, which is encapsulated within porous materials, can be described by the first-order equation.

$$F = 1 - e^{-kt} \qquad (2)$$

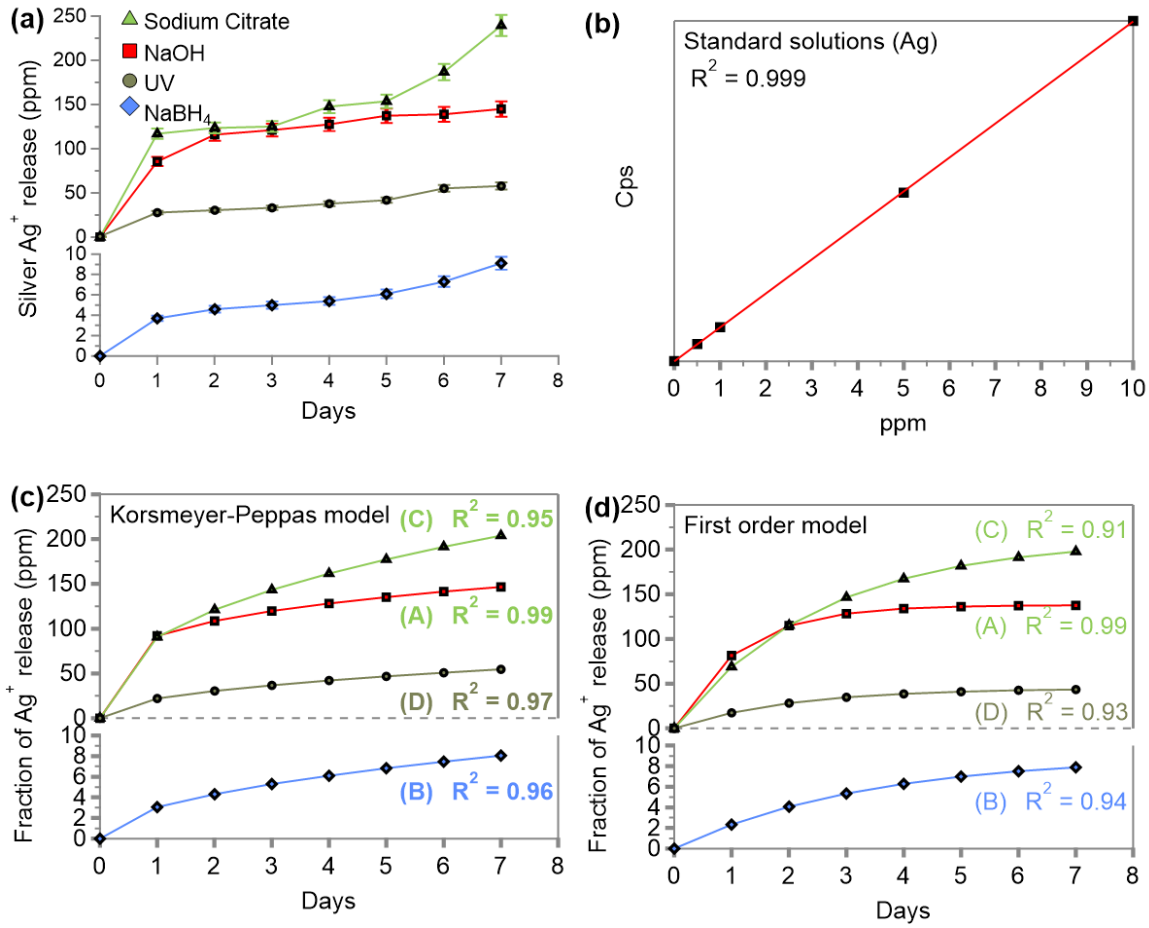

Figure 2—9: Silver release behavior of Ag doped MoO_3/PAN nanofiber membrane reduced with NaOH, $NaBH_4$, sodium citrate, and under UV light **(a)**, standard curve **(b)** and fitted curve of Ag-MoO_3/PAN nanofiber membranes **(c-d)**. The error bars correspond to the standard deviation of three measurements.

2.11 Antibacterial.

Inhibition zones are summarized in **Figure *2—10***, while their corresponding agar plate were shown. The observed inhibition zones indicate the effectiveness of Ag-MoO_3/PAN nanofibers in inhibiting the growth of both *E. coli* and *B subtilis* bacteria. The NaOH treated NFM possibly increased the surface roughening and porosity of the composite, which can enhance the contact between the material and bacteria[41]. The alkaline nature

might also support to the exposure of more active sites on the surface[42], which also promoting the release of silver ions, observed in silver released behavior .With $NaBH_4$ reducing agent might lead to the reduction of silver ions to metallic silver nanoparticles on the composite's surface which confirmed with XRD pattern. These nanoparticles have a large surface area, that could increase the potential for contact with bacterial cells. These interact with bacterial cell membranes, disrupting their integrity and causing leakage of cellular contents[43]. Sodium citrate treatment can act as a stabilizing agent, preventing the aggregation of silver nanoparticles which also promotes the release of silver ions. Dispersed nanoparticles which were also observed in FE-SEM offer a larger effective surface area for interactions with bacteria. In UV light treated sample could generate reactive oxygen species (ROS) on the surface of the composite, which have potent antibacterial effects by damaging bacterial DNA, proteins, and lipids.[44,45]All samples have different approach to destroy the bacteria in their vicinity area and the results indicate the broad-spectrum antibacterial potential of Ag-MoO_3/PAN nanofibers. These samples displaying considerable inhibition zones confirmed from previous report[39,46].

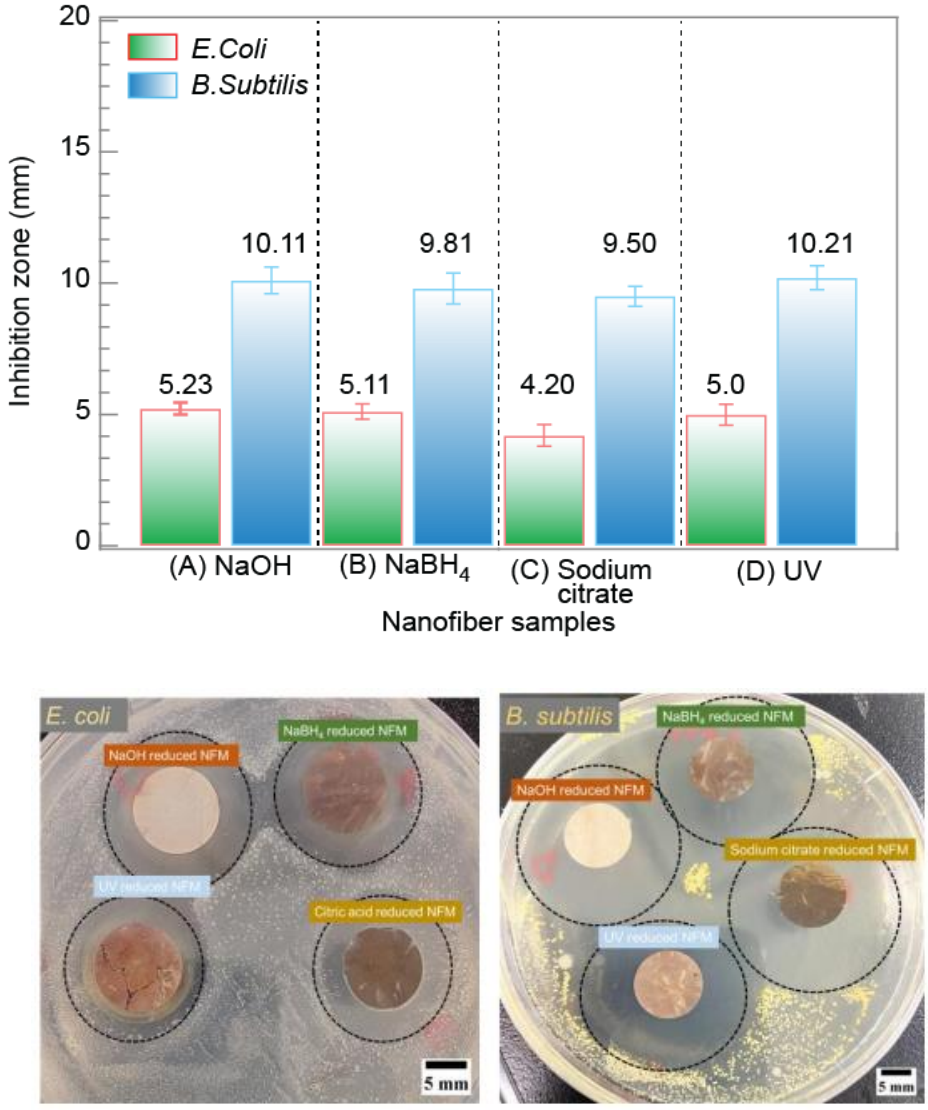

Figure 2—10: Zone of inhibition of Ag-MoO_3/PAN treated with different reducing agents and their corresponding agar plate.

2.12 Mechanical properties.

When applying wound dressings, it is essential to prioritize both strength and flexibility. The study examined the mechanical strength of two types of nanofibers: blank PAN and MoO_3/PAN (as seen in **Figure *2—11***). The results revealed that blank PAN nanofibers displayed the highest tensile strength at 6.4 MPa with 44% elongation, while MoO_3/PAN nanofibers had a tensile strength of 1.7 MPa and 44% elongation, showing

approximately 73% lower strength compared to blank PAN nanofibers. Materials with lower stress values tend to exhibit improved elasticity and reduced rigidity, allowing them to better adapt to the contours of the wound and surrounding skin[47].

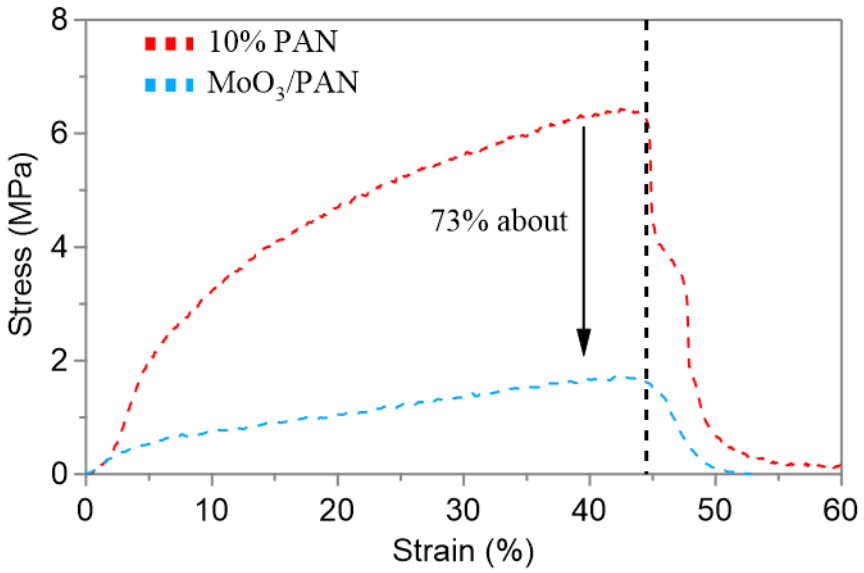

Figure 2—11: Stress-strain curves of the polyacrylonitrile and MoO_3/PAN nanofiber membrane.

2.13 Conclusion:

In summary, we synthesized a polyacrylonitrile nanofiber with incorporation of molybdenum oxide nanoparticles. As synthesized MoO_3/PAN NFMs were treated with four different reducing agents (NaOH, $NaBH_4$, sodium citrate, and UV light) provide valuable insights into their potential applications in wound dressing. The water contact angle increases about 49% in NaOH treated sample as compared with other reducing agents, which are almost same values. This led to a less wettable surface, potentially beneficial for creating a hydrophobic barrier that repels water and prevents excessive moisture buildup. While the $NaBH_4$, sodium citrate, and UV treated samples are more wettable surfaces, promoting better fluid absorption and contact with the wound bed. The antibacterial inhibition zone results highlight the antimicrobial properties of the nanofibers. All samples demonstrate significant inhibition zones against both *E. coli* and *B. subtilis*, indicating strong antibacterial activity. One of the intriguing observations is that the UV-treated samples exhibited a significantly lower number of silver nanoparticles attached to the surface but demonstrate 1.5% higher inhibition zones compared to the other samples.

The silver release profiles demonstrate sustained release of silver ions from the nanofibers over time. Among the treatments, sodium citrate exhibited the highest silver release, reaching 239.3 ppm over a period of 7 days. In contrast, the lowest silver release was observed in the $NaBH_4$ treated samples, which were approximately 96% lower in 7 days compared to the silver release from sodium citrate-treated samples. Comparing the four reducing agents, NaOH treated sample stands out with significant antibacterial activity and a hydrophobic surface. $NaBH_4$ treatment shows moderate antibacterial activity and enhanced wettability. Sodium citrate processed sample exhibits

mild antibacterial activity and enhanced wettability with a higher rate of silver ion release. UV light treatment of the sample offers strong antimicrobial activity and sustained silver ion release. Remarkably, both polyacrylonitrile and MoO_3/PAN composites exhibited an identical strain value of 45% when subjected to stress. However, MoO_3/PAN displayed a substantially lower stress value, being 73% less than that of the blank PAN nanofiber. The choice of the best treatment for wound dressing depends on specific wound characteristics and individual patient needs. Nanofiber treated with NaOH might be suitable for wounds requiring a drier healing environment. While $NaBH_4$ treatment can benefit wounds with moderate exudate levels, requiring better fluid absorption. In Sodium citrate treated sample may be suitable for wounds with minimal exudate levels, requiring a balance between moisture retention and fluid absorption. UV light exposure nanofiber can be considered for wounds prone to infection.

References:

(1) Brodell, L. A.; Rosenthal, K. S. Skin Structure and Function. *Infect. Dis. Clin. Pract.* **2008**, *16* (2), 113–117. https://doi.org/10.1097/IPC.0b013e3181660bf4.

(2) Dreifke, M. B.; Jayasuriya, A. A.; Jayasuriya, A. C. Current Wound Healing Procedures and Potential Care. *Mater. Sci. Eng. C* **2015**, *48*, 651–662. https://doi.org/10.1016/j.msec.2014.12.068.

(3) He, X.; Qian, Y.; Wu, C.; Feng, J.; Sun, X.; Zheng, Q.; Li, X.; Shen, J. Entropy-Mediated High-Entropy MXenes Nanotherapeutics: NIR-II-Enhanced Intrinsic Oxidase Mimic Activity to Combat Methicillin-Resistant Staphylococcus Aureus Infection. *Adv. Mater.* **2023**, *2211432*, 1–17. https://doi.org/10.1002/adma.202211432.

(4) Serag, E.; El-Aziz, A. M. A.; El-Maghraby, A.; Taha, N. A. Electrospun Non-Wovens Potential Wound Dressing Material Based on Polyacrylonitrile/Chicken Feathers Keratin Nanofiber. *Sci. Rep.* **2022**, *12* (1), 15460. https://doi.org/10.1038/s41598-022-19390-3.

(5) Haider, M. K.; Ullah, A.; Sarwar, M. N.; Saito, Y.; Sun, L.; Park, S.; Kim, I. S. Lignin-Mediated in-Situ Synthesis of CuO Nanoparticles on Cellulose Nanofibers: A Potential Wound Dressing Material. *Int. J. Biol. Macromol.* **2021**, *173*, 315–326. https://doi.org/10.1016/j.ijbiomac.2021.01.050.

(6) Lv, H.; Cui, S.; Yang, Q.; Song, X.; Wang, D.; Hu, J.; Zhou, Y.; Liu, Y. AgNPs-Incorporated Nanofiber Mats: Relationship between AgNPs Size/Content, Silver Release, Cytotoxicity, and Antibacterial Activity. *Mater. Sci. Eng. C* **2021**, *118*, 111331. https://doi.org/10.1016/j.msec.2020.111331.

(7) Abdo, H. S.; Khalil, K. A.; Al-Deyab, S. S.; Altaleb, H.; Sherif, E. S. M. Antibacterial Effect of Carbon Nanofibers Containing Ag Nanoparticles. *Fibers Polym.* **2013**, *14* (12), 1985–1992. https://doi.org/10.1007/s12221-013-1985-3.

(8) Daeschlein, G. Antimicrobial and Antiseptic Strategies in Wound Management. *Int. Wound J.* **2013**, *10* (s1), 9–14. https://doi.org/10.1111/iwj.12175.

(9) Félix, G.; Soto-Robles, C. A.; Nava, E.; Lugo-Medina, E. Principal Metabolites in Extracts of Different Plants Responsible for Antibacterial Effects. *Chem. Res. Toxicol.* **2021**, *34* (9), 1970–1983. https://doi.org/10.1021/acs.chemrestox.1c00161.

(10) Evans, S. M.; Cowan, M. M. Plant Products as Antimicrobial Agents. *Cosmet. Drug Microbiol.* **2016**, *12* (4), 205–231. https://doi.org/10.3109/9781420019919-17.

(11) Ribeiro, A. I.; Dias, A. M.; Zille, A. Synergistic Effects between Metal Nanoparticles and Commercial Antimicrobial Agents: A Review. *ACS Appl. Nano Mater.* **2022**, *5* (3), 3030–3064. https://doi.org/10.1021/acsanm.1c03891.

(12) Mijnendonckx, K.; Leys, N.; Mahillon, J.; Silver, S.; Van Houdt, R. Antimicrobial Silver: Uses, Toxicity and Potential for Resistance. *BioMetals* **2013**, *26* (4), 609–621. https://doi.org/10.1007/s10534-013-9645-z.

(13) Nishimura, S.; Mott, D.; Takagaki, A.; Maenosono, S.; Ebitani, K. Role of Base in the Formation of Silver Nanoparticles Synthesized Using Sodium Acrylate as a Dual Reducing and Encapsulating Agent. *Phys. Chem. Chem. Phys.* **2011**, *13* (20), 9335–9343. https://doi.org/10.1039/c0cp02985h.

(14) Li, Y.; Song, Q.; Fan, B.; Zhang, R. Effects of Reducing Agents on the Synthesis of Ag/RGO Nanocomposites. *Mater. Res. Express* **2017**, *4* (1), 015014.

https://doi.org/10.1088/2053-1591/aa522e.

(15) Roto, R.; Rasydta, H. P.; Suratman, A.; Aprilita, N. H. Effect of Reducing Agents on Physical and Chemical Properties of Silver Nanoparticles. *Indones. J. Chem.* **2018**, *18* (4), 614–620. https://doi.org/10.22146/ijc.26907.

(16) Liao, G.; Gong, Y.; Zhong, L.; Fang, J.; Zhang, L.; Xu, Z.; Gao, H.; Fang, B. Unlocking the Door to Highly Efficient Ag-Based Nanoparticles Catalysts for NaBH4-Assisted Nitrophenol Reduction. *Nano Res.* **2019**, *12* (10), 2407–2436. https://doi.org/10.1007/s12274-019-2441-5.

(17) Phuruangrat, A.; Keereesaensuk, P. O.; Karthik, K.; Dumrongrojthanath, P.; Ekthammathat, N.; Thongtem, S.; Thongtem, T. Synthesis of Ag/Bi2MoO6 Nanocomposites Using NaBH4 as Reducing Agent for Enhanced Visible-Light-Driven Photocatalysis of Rhodamine B. *J. Inorg. Organomet. Polym. Mater.* **2020**, *30* (2), 322–329. https://doi.org/10.1007/s10904-019-01190-4.

(18) Phan, D.-N.; Dorjjugder, N.; Saito, Y.; Taguchi, G.; Lee, H.; Lee, J. S.; Kim, I.-S. The Mechanistic Actions of Different Silver Species at the Surfaces of Polyacrylonitrile Nanofibers Regarding Antibacterial Activities. *Mater. Today Commun.* **2019**, *21* (August), 100622. https://doi.org/10.1016/j.mtcomm.2019.100622.

(19) Husanu, E.; Chiappe, C.; Bernardini, A.; Cappello, V.; Gemmi, M. Synthesis of Colloidal Ag Nanoparticles with Citrate Based Ionic Liquids as Reducing and Capping Agents. *Colloids Surfaces A Physicochem. Eng. Asp.* **2018**, *538*, 506–512. https://doi.org/10.1016/j.colsurfa.2017.11.033.

(20) Ranoszek-Soliwoda, K.; Tomaszewska, E.; Socha, E.; Krzyczmonik, P.; Ignaczak, A.; Orlowski, P.; Krzyzowska, M.; Celichowski, G.; Grobelny, J. The

Role of Tannic Acid and Sodium Citrate in the Synthesis of Silver Nanoparticles. *J. Nanoparticle Res.* **2017**, *19* (8), 273. https://doi.org/10.1007/s11051-017-3973-9.

(21) Park, H. H.; Park, H. H.; Zhang, X.; Choi, Y. J.; Kim, H.; Hill, R. H. Facile Synthesis and Size Control of Ag Nanoparticles by a Photochemical Reduction at Room Temperature. *J. Ceram. Soc. Japan* **2010**, *118* (1383), 1002–1005. https://doi.org/10.2109/jcersj2.118.1002.

(22) Bastús, N. G.; Merkoçi, F.; Piella, J.; Puntes, V. Synthesis of Highly Monodisperse Citrate-Stabilized Silver Nanoparticles of up to 200 Nm: Kinetic Control and Catalytic Properties. *Chem. Mater.* **2014**, *26* (9), 2836–2846. https://doi.org/10.1021/cm500316k.

(23) Phan, D. N.; Dorjjugder, N.; Saito, Y.; Taguchi, G.; Ullah, A.; Kharaghani, D.; Kim, I. S. The Synthesis of Silver-Nanoparticle-Anchored Electrospun Polyacrylonitrile Nanofibers and a Comparison with as-Spun Silver/Polyacrylonitrile Nanocomposite Membranes upon Antibacterial Activity. *Polym. Bull.* **2020**, *77* (8), 4197–4212. https://doi.org/10.1007/s00289-019-02969-8.

(24) Niu, Z.; Zhou, C.; Wang, J.; Xu, Y.; Gu, C.; Jiang, T.; Zeng, S.; Zhang, Y.; Ang, D. S.; Zhou, J. UV-Light-Assisted Preparation of MoO3−x/Ag NPs Film and Investigation on the SERS Performance. *J. Mater. Sci.* **2020**, *55* (21), 8868–8880. https://doi.org/10.1007/s10853-020-04669-5.

(25) Tian, K.; Wei, L.; Zhang, X.; Jin, Y.; Guo, X. Membranes of Carbon Nanofibers with Embedded MoO3 Nanoparticles Showing Superior Cycling Performance for All-Solid-State Flexible Supercapacitors. *Mater. Today Energy* **2017**, *6*, 27–35.

https://doi.org/10.1016/j.mtener.2017.08.004.

(26) Mu, J.; Guan, Y.; Wang, L.; Li, H.; Liu, Y.; Che, H.; Liu, A.; Guo, Z.; Zhang, X.; Zhang, Z. Flexible Heat-Treated PAN Nanofiber/MoO 2 /MoS 2 Composites as High Performance Supercapacitor Electrodes. *J. Mater. Sci. Mater. Electron.* **2019**, *30* (9), 8210–8219. https://doi.org/10.1007/s10854-019-01136-z.

(27) Zollfrank, C.; Gutbrod, K.; Wechsler, P.; Guggenbichler, J. P. Antimicrobial Activity of Transition Metal Acid MoO3 Prevents Microbial Growth on Material Surfaces. *Mater. Sci. Eng. C* **2012**, *32* (1), 47–54. https://doi.org/10.1016/j.msec.2011.09.010.

(28) Guggenbichler, J.K., Eberhardt, N., Martinez, H.P., Wildner, H. Substance with an Antimicrobial Effect. PCT/EP2007/009814, 2007.

(29) Vempati, S.; Ranjith, K. S.; Topuz, F.; Biyikli, N.; Uyar, T. Electrospinning Combined with Atomic Layer Deposition to Generate Applied Nanomaterials: A Review. *ACS Appl. Nano Mater.* **2020**, *3* (7), 6186–6209. https://doi.org/10.1021/acsanm.0c01120.

(30) Wei, Z.; Gong, P.; Kong, X.; Li, M.; Cheng, J.; Zhou, H.; Li, D.; Ye, Y.; Lu, X.; Yu, J.; Lu, S. Enhanced Thermal Conductivity of Nanodiamond Nanosheets/Polymer Nanofiber Composite Films by Uniaxial and Coaxial Electrospinning: Implications for Thermal Management of Nanodevices. *ACS Appl. Nano Mater.* **2023**, *6* (10), 8358–8366. https://doi.org/10.1021/acsanm.3c00591.

(31) Zhang, H.; Wang, F.; Nestler, B. Janus Droplet Formation via Thermally Induced Phase Separation: A Numerical Model with Diffusion and Convection. *Langmuir* **2022**, *38* (22), 6882–6895. https://doi.org/10.1021/acs.langmuir.2c00308.

(32) McShan, D.; Ray, P. C.; Yu, H. Molecular Toxicity Mechanism of Nanosilver. *J. Food Drug Anal.* **2014**, *22* (1), 116–127. https://doi.org/10.1016/j.jfda.2014.01.010.

(33) Kostenko, V.; Lyczak, J.; Turner, K.; Martinuzzi, R. J. Impact of Silver-Containing Wound Dressings on Bacterial Biofilm Viability and Susceptibility to Antibiotics during Prolonged Treatment. *Antimicrob. Agents Chemother.* **2010**, *54* (12), 5120–5131. https://doi.org/10.1128/AAC.00825-10.

(34) Leaper, D. Appropriate Use of Silver Dressings in Wounds: International Consensus Document. *Int. Wound J.* **2012**, *9* (5), 461–464. https://doi.org/10.1111/j.1742-481X.2012.01091.x.

(35) Hartati, S.; Zulfi, A.; Maulida, P. Y. D.; Yudhowijoyo, A.; Dioktyanto, M.; Saputro, K. E.; Noviyanto, A.; Rochman, N. T. Synthesis of Electrospun PAN/TiO 2 /Ag Nanofibers Membrane As Potential Air Filtration Media with Photocatalytic Activity. *ACS Omega* **2022**, *7* (12), 10516–10525. https://doi.org/10.1021/acsomega.2c00015.

(36) Pan, S. F.; Ke, X. X.; Wang, T. Y.; Liu, Q.; Zhong, L. Bin; Zheng, Y. M. Synthesis of Silver Nanoparticles Embedded Electrospun PAN Nanofiber Thin-Film Composite Forward Osmosis Membrane to Enhance Performance and Antimicrobial Activity. *Ind. Eng. Chem. Res.* **2019**, *58* (2), 984–993. https://doi.org/10.1021/acs.iecr.8b04893.

(37) Bernard, J. J.; Gallo, R. L.; Krutmann, J. Photoimmunology: How Ultraviolet Radiation Affects the Immune System. *Nat. Rev. Immunol.* **2019**, *19* (11), 688–701. https://doi.org/10.1038/s41577-019-0185-9.

(38) Rezaie, A.; Leite, G. G. S.; Melmed, G. Y.; Mathur, R.; Villanueva-Millan, M. J.;

Parodi, G.; Sin, J.; Germano, J. F.; Morales, W.; Weitsman, S.; Kim, S. Y.; Park, J. H.; Sakhaie, S.; Pimentel, M. Ultraviolet A Light Effectively Reduces Bacteria and Viruses Including Coronavirus. *PLoS One* **2020**, *15* (7), e0236199. https://doi.org/10.1371/journal.pone.0236199.

(39) Singh, S.; Rai, N.; Tiwari, H.; Gupta, P.; Verma, A.; Kumar, R.; Kailashiya, V.; Salvi, P.; Gautam, V. Recent Advancements in the Formulation of Nanomaterials-Based Nanozymes, Their Catalytic Activity, and Biomedical Applications. *ACS Appl. Bio Mater.* **2023**. https://doi.org/10.1021/acsabm.3c00253.

(40) Lu, D. R.; Abu-Izza, K.; Mao, F. Nonlinear Data Fitting for Controlled Release Devices: An Integrated Computer Program. *Int. J. Pharm.* **1996**, *129* (1–2), 243–251. https://doi.org/10.1016/0378-5173(95)04356-X.

(41) Li, J.; Wu, X.; Liang, Z.; Wei, Z.; Chen, Z.; Wang, Y.; Li, W.; Zhang, W.; Yang, R.; Qiu, H.; Li, X.; Li, Q.; Chen, J. A Programmed Surface on Dental Implants Sequentially Initiates Bacteriostasis and Osseointegration. *Colloids Surfaces B Biointerfaces* **2023**, *230* (July), 113477. https://doi.org/10.1016/j.colsurfb.2023.113477.

(42) Ping, M. M.; Qiu, S. J.; Wei, G. J.; Liu, J. X.; Wang, Z. J.; Wang, S. T.; An, C. H. Monolith Free-Standing Plasmonic PAN/Ag/AgX (X = Br, I) Nanofiber Mat as Easily Recoverable Visible-Light-Driven Photocatalyst. *Rare Met.* **2019**, *38* (5), 361–368. https://doi.org/10.1007/s12598-019-01242-1.

(43) Wang, L.; Hu, C.; Shao, L. The-Antimicrobial-Activity-of-Nanoparticles--Present-Situati. *Int. J. Nanomedicine* **2017**, *12*, 1227–1249.

(44) Hwang, C.; Choi, M. H.; Kim, H. E.; Jeong, S. H.; Park, J. U. Reactive Oxygen

Species-Generating Hydrogel Platform for Enhanced Antibacterial Therapy. *NPG Asia Mater.* **2022**, *14* (1). https://doi.org/10.1038/s41427-022-00420-5.

(45) Vatansever, F.; de Melo, W. C. M. A.; Avci, P.; Vecchio, D.; Sadasivam, M.; Gupta, A.; Chandran, R.; Karimi, M.; Parizotto, N. A.; Yin, R.; Tegos, G. P.; Hamblin, M. R. Antimicrobial Strategies Centered around Reactive Oxygen Species – Bactericidal Antibiotics, Photodynamic Therapy, and Beyond. *FEMS Microbiol. Rev.* **2013**, *37* (6), 955–989. https://doi.org/10.1111/1574-6976.12026.

(46) Yuan, H.; Chen, L.; Hong, F. F. A Biodegradable Antibacterial Nanocomposite Based on Oxidized Bacterial Nanocellulose for Rapid Hemostasis and Wound Healing. *ACS Appl. Mater. Interfaces* **2020**, *12* (3), 3382–3392. https://doi.org/10.1021/acsami.9b17732.

(47) Kwan, A. L.; Lin, C. L.; Yanamoto, H.; Howng, S. L.; Kassell, N. F.; Lee, K. S. Systemic Administration of the Potassium Channel Activator Cromakalim Attenuates Cerebral Vasospasm after Experimental Subarachnoid Hemorrhage. *Neurosurgery* **1998**, *42* (2), 347–351. https://doi.org/10.1097/00006123-199802000-00085.

CHAPTER 3. Enhancement of antibacterial properties and control silver release behavior by hybrid MoO_3/PAN composite membrane with rapid silver reduction.

3.1 Introduction

The main purpose of wound dressing is to create a healing environment for wounds while protecting them from damage and the invasion of harmful microorganisms. Whether it's a sutured wound resulting from surgery or trauma or an open wound preventing infections is a concern in wound care worldwide[1,2]. However, addressing infection control has become an issue due to the increasing number of microorganisms. Many bacteria have developed resistance to antibiotics, which focuses on the need to explore new materials for treating harmful microorganisms[3–5]. Reduction in the production of new antibiotics material or reduce their usage, it's estimated that bacterial infections could cause around 10 million deaths by 2050[6]. Therefore, we must find new approaches to combat bacteria beyond relying on antibiotics. To tackle this challenge of preventing infections of microorganisms there has been active research in alternative antibacterial technologies that could replace conventional remedial treatment[7,8]. Unlike antiseptic drugs that attack sites within the cells, metal-containing nanomaterials possess inherent passive antibacterial mechanisms that make them less prone to resistance. These mechanisms involve direct interactions with microorganisms, the release of metal ions that generate reactive oxygen species (ROS), and the indirect enhancement of ROS production that helps to combat bacteria[7,9–11]. Moreover, these nanomaterials possess properties that can be easily modified and tailored according to needs making them more flexible compared to antibiotics. Despite the advantages of using metal-based nanomaterials for their passive anti-bacterial properties, they can still have some drawbacks. For instance, uncontrolled and sustained release of metal ions can lead to the development of excessive ROS, which can cause various diseases. Moreover, the rapid deterioration of these materials can decrease their effectiveness

over time[12–14].

To address this challenge, hybrid nanomaterials are being employed, which combine various nanomaterials to enhance antibacterial efficacy and mitigate the risk of resistance development[15]. By creating hybrid composites, it becomes possible to maximize the advantages while minimizing the drawbacks associated with individual types of nanoparticles (NPs). Additionally, the "combinatorial" approach allows for an extended duration of effective antibacterial action, significantly reducing bacterial resistance development[10,16]. Among the diverse array of nanomaterials available, organic polymerized nanomaterials offer the advantage of pH-responsive antimicrobial properties and the ability to mimic the actions of antimicrobial peptides to combat bacteria[17,18]. Inorganic metals[7] such as gold[19,20] (Au), silver[21,22] (Ag), and copper[23,24] (Cu), as well as transition metal dichalcogenides[25] (TMDs), metal oxides[26], carbon-based nanomaterials[27], polymers, and their nanocomposites have all been prominently utilized in the antibacterial research field[28]. These materials operate through distinct antibacterial mechanisms compared to conventional antibiotics and carry a reduced risk of fostering bacterial resistance. Consequently, the utilization of nanomaterials holds significant promise as an alternative to antibiotics for combating drug-resistant bacteria.

In various inorganic materials, molybdenum (Mo) based nanomaterials have gained significant attention in the antibacterial research field due to their distinctive physicochemical properties[29,30]. Mo also serves as an essential trace element for microorganisms, plants, and animals[9]. Furthermore, within organisms, Mo functions as a cofactor for numerous enzymes (such as aldehyde, xanthine, and sulphite oxidase), participating in metabolic processes and facilitating various physiological functions, including protein synthesis[31,32]. One highly promising antibacterial nanomaterial is

molybdenum trioxide (MoO_3)[33]. Its antimicrobial mechanism in the presence of water involves a dissolving process, resulting in an acidic reaction and the formation of hydronium (H_3O^+) and molybdate (MoO_4^{2-}) ions. The infiltration of hydronium (H_3O^+) ion through the bacterial cell wall disrupts the pH balance, enzyme activity, and transport systems within the cell. This acidic, low-pH environment induced by MoO_3 nanoparticles has been reported as an effective antimicrobial agent against susceptible and resistant strains of bacteria[34]. The penetration of hydroxonium ions through cell membranes hindered cell proliferation, affecting enzymes and transport systems, thereby slowing down the growth of bacteria and fungi[35].

In addition to its antibacterial properties, MoO_{3-x} can also be combined with other materials to synthesize functionalized nanocomposites, which can generate synergistic antibacterial effects[36]. Silver ions Ag^+ have long been recognized as effective antimicrobial agents with low toxicity to humans and extensively studied in various in vitro and in vivo applications[37]. Silver molybdates have been explored in fields such as lubrication[38], humidity[38], gas sensors[38], photoelectronic devices[38], and surface-enhanced Raman scattering techniques[39]. While the release of Ag^+ in wound dressings is a common practice with several benefits in wound care, it's crucial to control the release to prevent potential harm from excessive Ag^+ release[12,40].

In addressing the issue of excessive silver ion release and its potential environmental impact, the molybdenum-PAN (MoO_3/PAN) membrane can serve as a key element to absorb and sequester these silver ions, preventing their release into the environment[41]. Additionally, it can create a moderate moist wound-healing environment while effectively controlling the release of silver ions to achieve antibacterial effects[42]. Previous research conducted by our team has confirmed the efficacy of molybdenum

trioxide nanoparticles (NPs) embedded in polyacrylonitrile (PAN) in promoting wound healing and controlling the release of silver ions for antibacterial purposes[43]. Notably, these NPs have exhibited highly promising antimicrobial properties against both *B. subtilis* and *E. coli*.

In this current study, we introduce a novel hybrid composite named the MoO_3/PAN membrane, which doped silver nanoparticles through a green fast synthesis approach mediated by UV light. To assess the antibacterial efficacy of this nanocomposite, we employed representative bacterial models, including *Escherichia coli* and *Bacillus subtilis*. That revealed a correlation between the silver content of the nanocomposites and their antibacterial effectiveness. Furthermore, we assessed controlled silver ion release, a crucial aspect of this research. These findings illustrate an outstanding advancement in the field of antibacterial materials and hold the potential to revolutionize wound dressings. A graphical representation of this study is shown in **Figure *3—1*** .

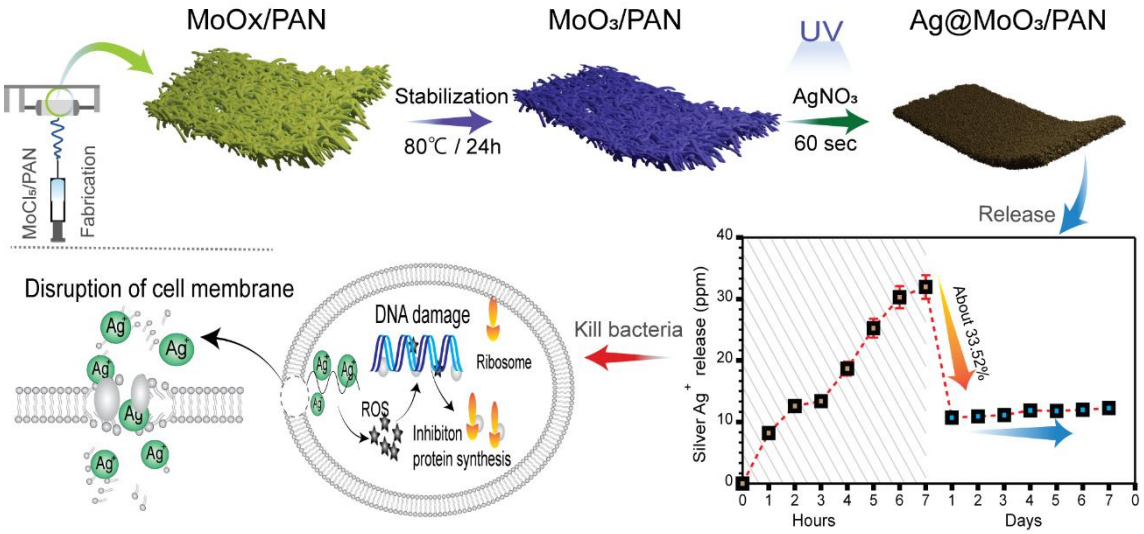

Figure 3—1: Graphical representation of silver nanoparticles doped on the surface of MoO_3/PAN composite membrane with silver release profile, and schematic illustration of bacterial death with silver ions.

3.2 Membrane fabrication

For the synthesis of the MoO_3-Polyacrylonitrile (PAN) composite membrane, a typical procedure was employed. Illustration was shown in **Figure *3—2***. Initially, a solution was prepared by dissolving 10% PAN in 10 cm^3 of dimethylformamide (DMF), resulting in a transparent solution. Subsequently, 60% molybdenum pentachloride ($MoCl_5$) relative to the polymer content was introduced into the 10% polymer solution with vigorous stirring. The reaction took place under ambient conditions, where the presence of atmospheric oxygen and residual water in DMF facilitated the oxidation and hydration of $MoCl_5$ precursors. During the initial 3 minutes of the reaction, the generation of white smoke, primarily composed of hydrogen chloride (HCl) gas, was observed continuously. Within 5 minutes, the solution underwent a transition from being colorless to exhibiting a jacinth hue, and eventually transformed into a blue coloration. This change in color was attributed to the formation of numerous small clusters of MoO_3. Once the dispersion process was complete, the solution was loaded into a 10 mL plastic syringe equipped with a needle having a diameter of 0.7 mm. The syringe pump was operated at a flow rate of 0.8 mL h^{-1}, with the collector positioned at 18.0 cm from the needle. An applied voltage of 20 kV was maintained throughout the process. The humidity was controlled at 40 ± 5%. The electrospun fibrous membranes initially appeared yellow in color. Subsequently, these membranes were carefully detached from the substrate and subjected to vacuum drying at 80 °C for a duration of 24 hours. This drying process served the dual purpose of removing DMF and enabling the formation of

a stable MoO_3/PAN membrane. Notably, this membrane underwent a color transition from yellow to blue during the drying process. The resultant, blue-colored nanofiber membranes were then ready for subsequent characterization and analysis. The photo-reduced, blue-colored membrane was submerged in a 0.1 M silver nitrate ($AgNO_3$) solution under UV light, leading to the spontaneous reduction and deposition of silver nanoparticles (AgNPs) onto the membrane. The rapid change in color, occurring within a minute as shown in the video W1, from blue to black served as confirmation of the successful deposition of AgNPs onto the membrane.

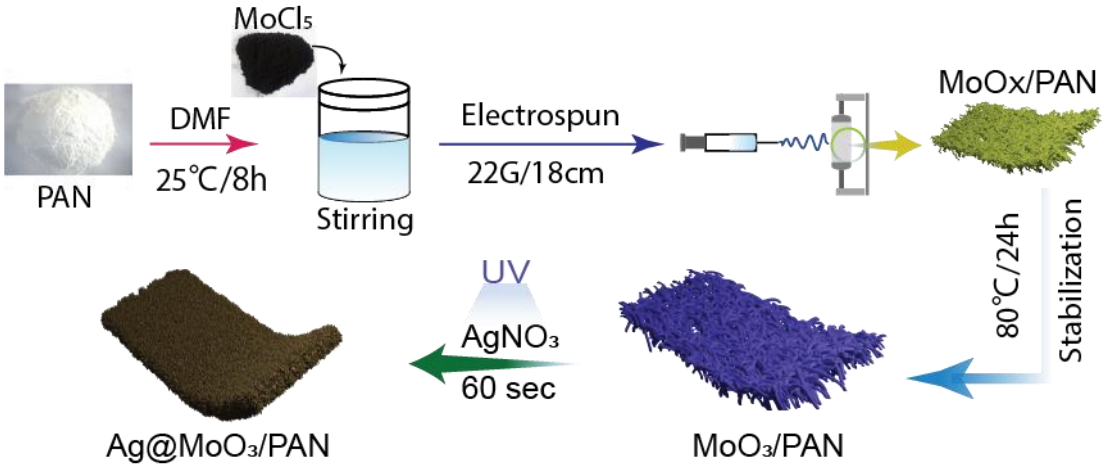

Figure 3—2: Graphical illustration of MoO_3/PAN membrane synthesis and Ag@MoO_3/PAN membrane fabrication.

3.3 Results and Discussion

The synthesis of the MoO_3/PAN composite membrane followed previous reports[44] on the WO_3/PAN membrane with slight modifications, as detailed in the experimental section of the supplementary material. The incorporation of silver into the MoO_3/PAN composite membrane was synthesized through a rapid within one-minute green synthesis method under UV light. The crystalline structures of both the MoO_3/PAN composite membrane, as shown in **Figure *3*—*3***a, and the Ag@MoO_3/PAN membrane,

displayed in **Figure *3*—*3***b, were analyzed using X-ray diffraction (XRD). In the MoO_3-PAN composite membrane, prominent peaks were observed at 9.6°, 16.69°, 19.30°, 25.65°, 29.25°, and 35.31°, corresponding to the (100), (110), (200), (210), (111), and (211) planes respectively. These findings align with the JCPDS reference number (JCPDS No. 00-065-0033) and confirm the molybdenum oxide membrane. After the introduction of silver nitrate ($AgNO_3$) into the MoO_3/PAN composite membrane under UV light, XRD analysis confirmed the conversion of ions into metallic silver. Strong corresponding peaks were observed at 27.21°, 32.03°, 33.49°, 38.87°, 48.09°, 51.22°, and 56.14°, corresponding to the (220), (311), (222), (400), (422), (511), and (440) planes of silver molybdenum oxide (Ag_2MoO_4). These peaks matched the JCPDS reference number (JCPDS No. 01-075-0250). Importantly, no additional peaks were observed, confirming the absence of other impurities, and attesting to the excellent crystalline quality of the Ag@MoO_3-PAN composite membrane. A typical polyacrylonitrile PAN peak was observed near 17.50° degree[45].

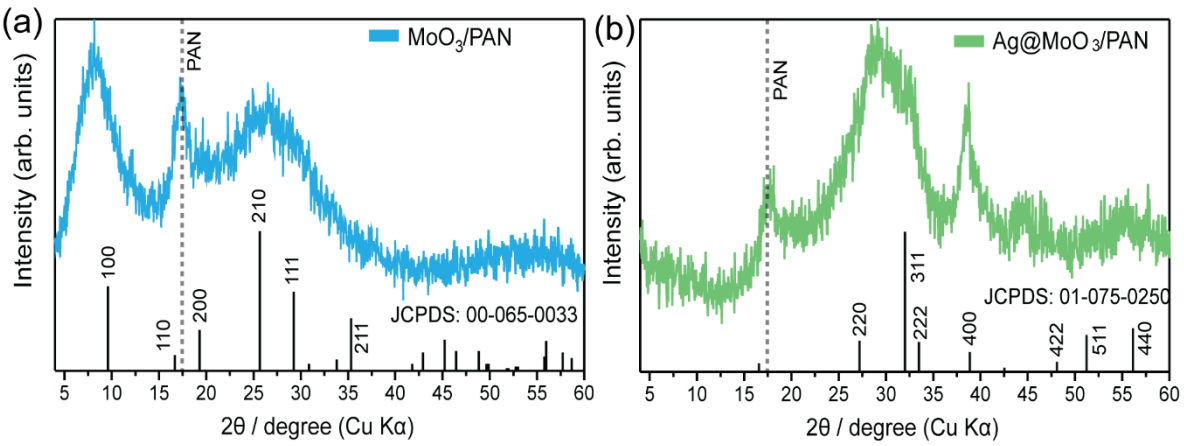

Figure 3—3: XRD diffraction patterns, with (a) representing the MoO_3/PAN composite membrane and (b) corresponding to the Ag@MoO_3/PAN membrane after silver doping.

The morphology of the MoO_3/PAN nanofiber composite was characterized using scanning electron microscopy (SEM), as depicted in **Figure *3*—*4***a, while **Figure *3*—*4***b illustrates the SEM analysis of the silver-deposited Ag@MoO_3/PAN membrane. SEM provides valuable insights into the membrane structure and their corresponding elemental distribution mappings. In the case of the MoO_3/PAN composite, the distribution of Mo and O elements appeared consistent and evenly dispersed, indicating a uniform mixture of the inorganic MoO_3 and organic components, resulting in a homogeneous phase. No other impurities were observed. Additionally, in the silver-deposited composite membrane, Ag was well-distributed across the membrane, as evidenced by the TEM image and elemental distribution, which revealed the presence of Mo, O, and Ag elements within the nanofibers. Furthermore, **Figure *3*—*4*** includes their Energy Dispersive X-ray Spectroscopy (EDS) spectra.

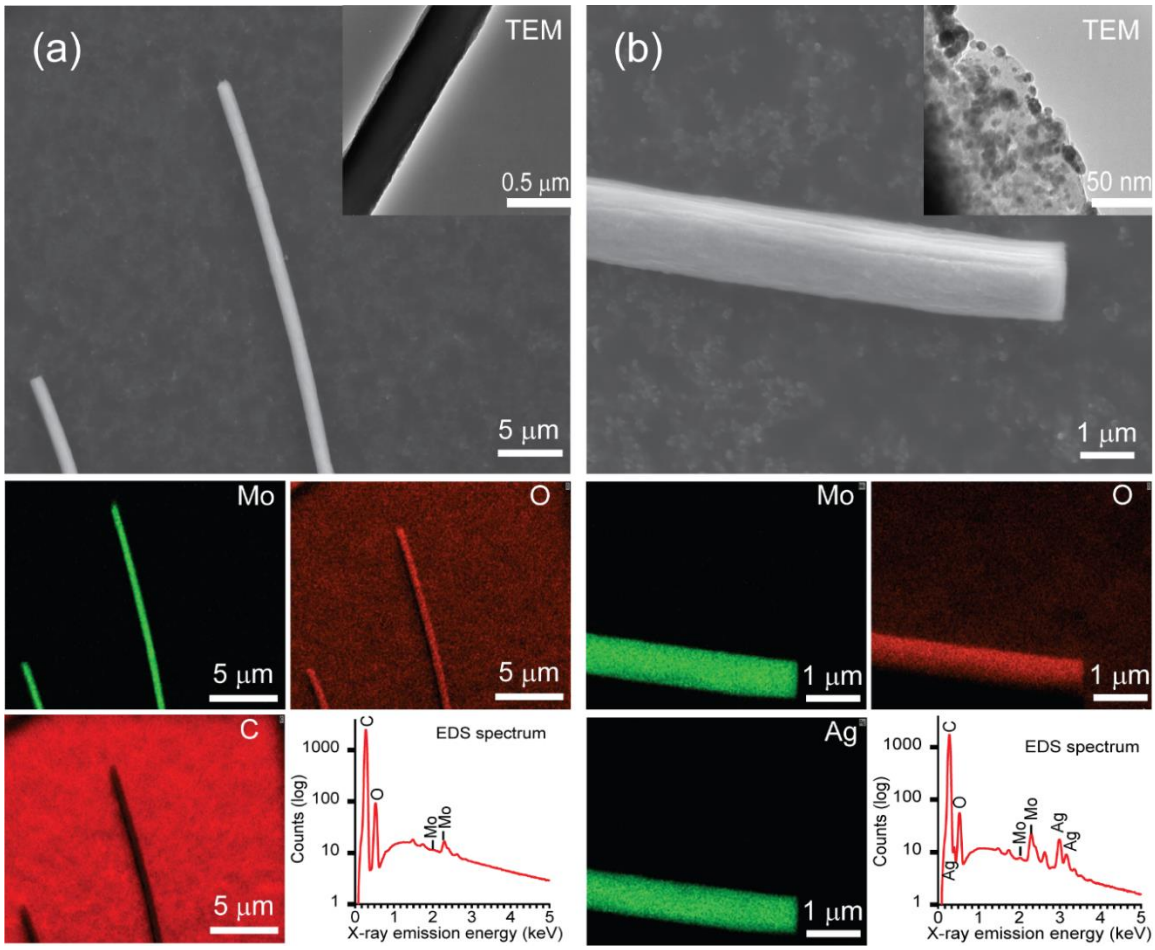

Figure 3—4: (a) SEM images of MoO_3/PAN and (b) SEM images of Ag@MoO_3/PAN nanofiber membrane, and their corresponding elemental mapping images of Mo, O, C, and Ag elements, and EDS spectrum and TEM images respectively.

3.4 XPS analysis

XSP was conducted to examine the surface elemental composition and chemical states of both the MoO_3/PAN membrane and the silver-doped composite membrane. The wideband spectra of both membranes, along with their corresponding Mo 3d and Ag 3d spectra, are depicted in **Figure *3*—*5***a-b. In the Mo 3d spectra of the membranes, it was observed that the Mo 3d doublet could be effectively fitted using a Gaussian function. The primary contributing peaks at 230.0 and 233.1 eV corresponded to the characteristic

values of the Mo^{5+} 3d doublet, and no minor peaks were detected. **Figure *3*—*5***c-d represent the Ag@MoO_3/PAN composite membrane, and their corresponding Mo 3d and Ag 3d spectra, respectively. The introduction of silver nanoparticles did not result in any noticeable shifts in the Mo spectrum, indicating that the presence of silver did not affect the transition state of molybdenum[43,46]. In the Ag 3d spectra, the major contributor peaks at 365.8 and 371.9 eV exhibited slight shifts in binding energy toward lower values. This shift was attributed to the reduction of silver ions to metallic silver (Ag^0). The dominant peaks confirmed the presence of metallic silver, while no minor peaks were observed, implying the complete reduction of silver ions to the metallic state[21] (Ag^0). A prominent oxygen peak, around 532 eV, was evident in both membranes, substantiating the formation of MoO_3 and $AgMoO_4$. Additionally, the N 1s spectrum was observed in the range of 397-399 eV, corresponding to the binding energies of Mo 3p and Mo-N, as well as amine N bonds. These results indicated that molybdenum was not only physically adsorbed but also chemically bonded with polyacrylonitrile (PAN), forming Mo-N bonds. Consequently, a coexistence of amorphous and crystalline structures was established[47].

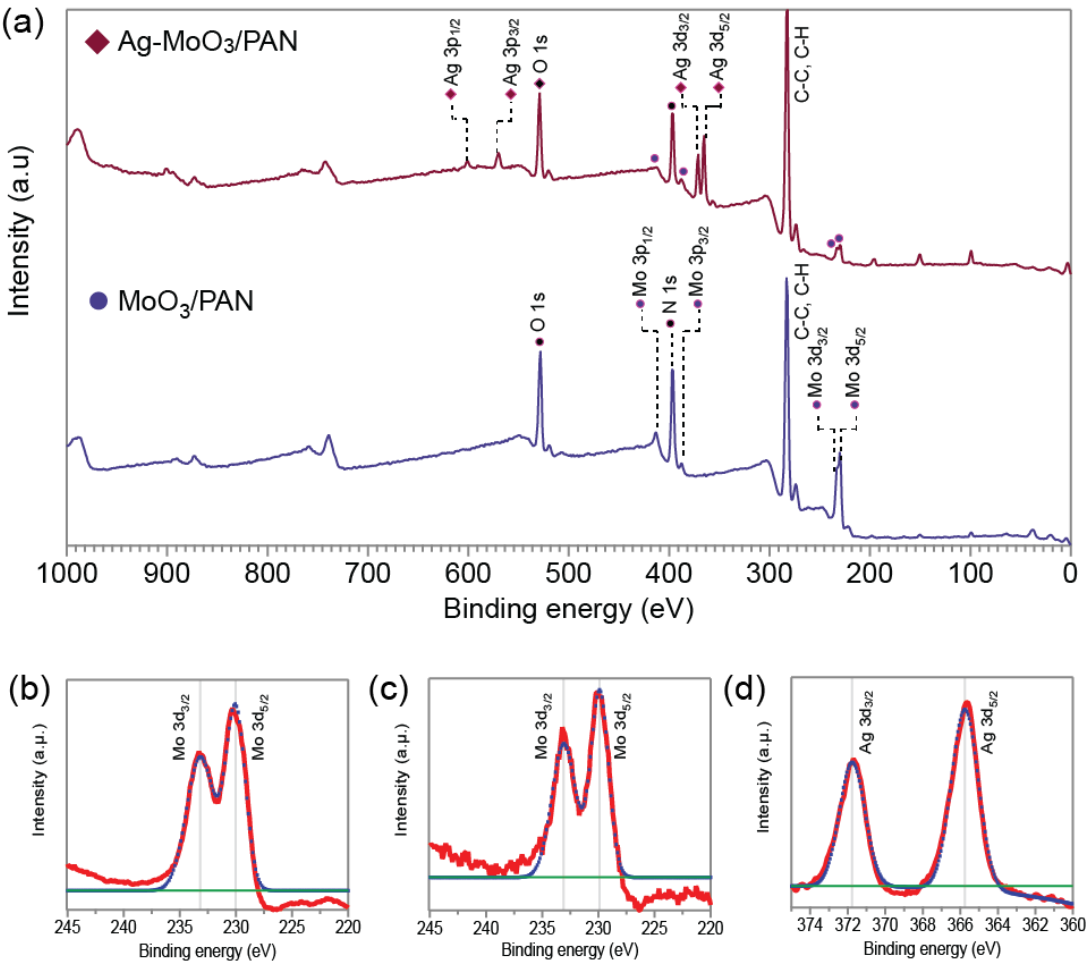

Figure 3—5: (a) Wide XPS spectrum of MoO_3/PAN and silver-doped membrane, High-resolution deconvoluted XPS spectrum for (b) Mo 3d for MoO_3/PAN membrane, (c) Mo 3d for Ag@MoO_3/PAN membrane and (d) Ag 3d for Ag@MoO_3/PAN membrane.

3.5 FT-IR spectra

FTIR were conducted in the range of 400-4000 cm^{-1} to identify various functional groups, as illustrated in **Figure *3—6***. The presence of the nitrile group (C≡N) in PAN is indicated by the peaks at 2242 cm^{-1}, while the bending and stretching vibrations of the C-H_2 functional group in PAN are represented by peaks at 1451 and 2918 cm^{-1}, respectively. Additionally, a weak ether peak (C-O-C) is observed at 1063 and 1249 cm^{-1}. Notably, the MoO_3 peak primarily appears below 1000 cm^{-1}. Peaks at 862 cm^{-1}

correspond to the bending vibrational modes of Mo-O-Mo, while the peak at 562 cm^{-1} is attributed to the stretching mode vibration of the Mo-O-Mo entity[47]. Small peak shifts are observed, potentially arising from the composite nature of the MoO_3/PAN membrane. Upon the introduction of Ag into the MoO_3/PAN membrane, significant changes occur, including the appearance of two new peaks at 1356 and 1619 cm^{-1}, accompanied by the disappearance of the Mo bending peak[47]. These changes suggest potential bonding interactions between molybdenum and silver[48].

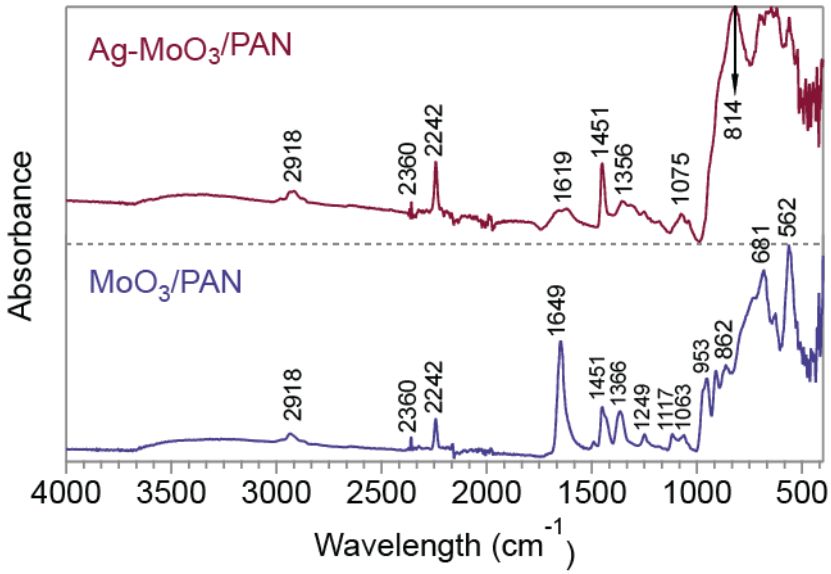

Figure 3—6: IR spectra of pristine MoO_3/PAN membrane and silver doped Ag@MoO_3/PAN membrane.

3.6 Thermal gravimetric analysis (TGA)

TGA of the molybdenum nanocomposite was shown in **Figure *3*—*7***a, revealing distinct two-step weight loss events in the as-prepared membrane. The initial small weight loss was due to the moisture evaporation. The initial weight loss occurring before 450°C is attributed to the decomposition of the PAN component, while the subsequent stages, ranging from 450 to 550°C, correspond to the dehydration and transformation of amorphous MoO_3 into a crystalline state[35]. Upon the introduction of

silver nanoparticles into the composite, as shown in **Figure *3*—*7***b, the T_g shifts towards 500°C. This shift in T_g towards a higher temperature range is attributed to increased lateral forces within the bulk state, which might be due to the restricted steric effect[49].

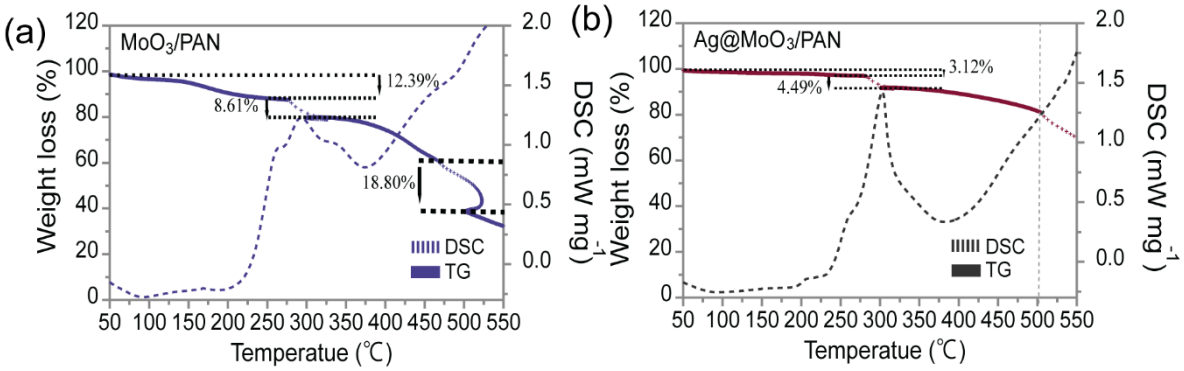

Figure 3—7: Thermogravimetric analysis of pure (a) MoO_3/PAN composite and (b) silver-doped composite membrane with their corresponding DSC curves respectively.

3.7 The BET analysis

BET of the as-prepared membrane was conducted using N_2 adsorption and desorption kinetics[50]. **Figure *3*—*8***a presents the BET surface area data. The surface area for MoO_3 measures approximately 13.25 m^2/g. Notably, upon the incorporation of silver nanoparticles into the membrane, the surface area increased by 23.89% as compared to the pristine MoO_3/PAN membrane. This enhancement of the area can be attributed to the enlargement of nanofiber diameter, as verified by SEM images larger nanofibers provide a greater surface area. There could be a chemical interaction of silver nanoparticles on the surface of the membrane, such as the adsorption of gas molecules onto the silver nanoparticles themselves[51]. The linear plot fit coefficient factor R^2 for the isotherm analysis was determined to be 0.991, indicating a good fit with the values displayed in **Figure *3*—*8***b.

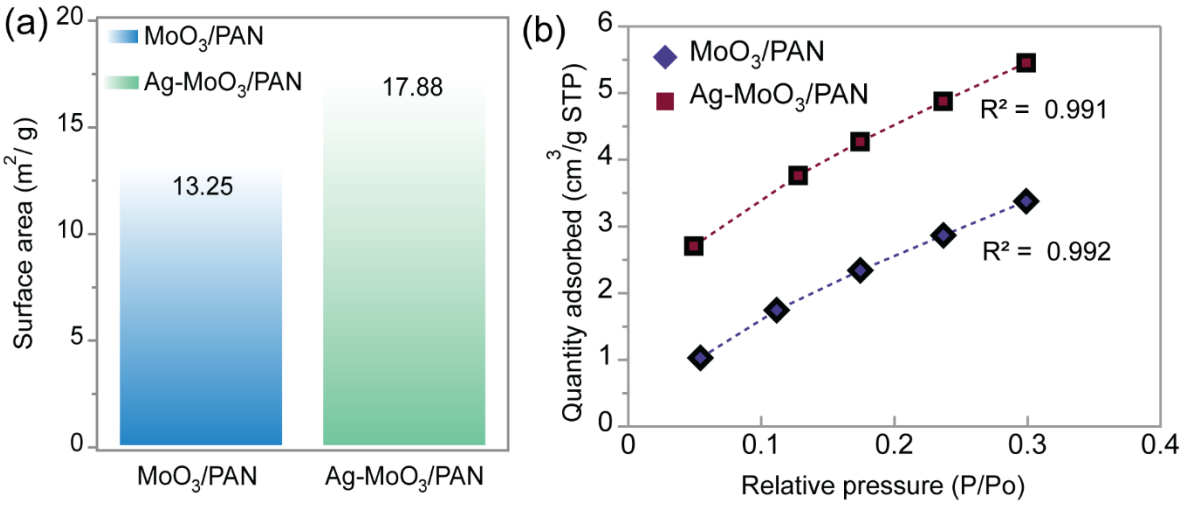

Figure 3—8: (a) BET surface area of both the MoO_3 and silver dopped membrane, (b) isotherm linear plot fit.

3.8 The DPPH antioxidant assay

Antioxidant for the prepared nanofiber membrane was conducted using the 2,2-diphenyl-1-picrylhydrazyl radical (DPPH) free radical scavenging method. To assess the antioxidant activity of the produced fibers, a 30 mg sample of the fiber was combined with 100 µl of DPPH solution in ethanol and 80 µl of assay buffer. This mixture was then incubated for various time intervals: specifically, 0.5 hours, 1 hour, 2 hours, 3 hours, 4 hours, 5 hours, 6 hours, and 7 hours. After each specified incubation period, the absorbance at 517 nm was measured using a UV–vis spectrophotometer (Lambda 900, PerkinElmer, USA). The DPPH free radical scavenging activity was calculated as a percentage using Equation 1[52].

$$\text{Scavenging activity (\%)} = \frac{Ac - As}{Ac} \times 100 \qquad (1)$$

Where As (sample) and Ac (control) are the absorption of DPPH with and without nanofiber membranes.

Figure *3—9* presents the assessment of the antioxidant activity of the prepared

MoO_3/PAN nanofiber membranes, utilizing ethanol as the solvent for the DPPH scavenging assay. MoO_3, as a composite material, is recognized for its antioxidant properties[31,53], yielding an initial activity of approximately 62% after a 30-minute evaluation. Interestingly, after 7 hours, this percentage only increased by 2% compared to the initial 30-minute measurement. Conversely, the silver doped MoO_3 composite membrane initially exhibited relatively low antioxidant activity, measuring approximately 15%. This reduction in activity could potentially be attributed to the presence of silver metal incorporated into the MoO_3 composite material[54]. Indeed, it seemed that the presence of silver applied an inhibitory effect on the antioxidant activity of MoO_3/PAN, possibly involving chemical interactions with the MoO_3/PAN components. Over time, the scavenging activity increased by approximately 30%, which may be associated with the gradual release of silver ions and potential oxidation of the DPPH molecules themselves[55,56].

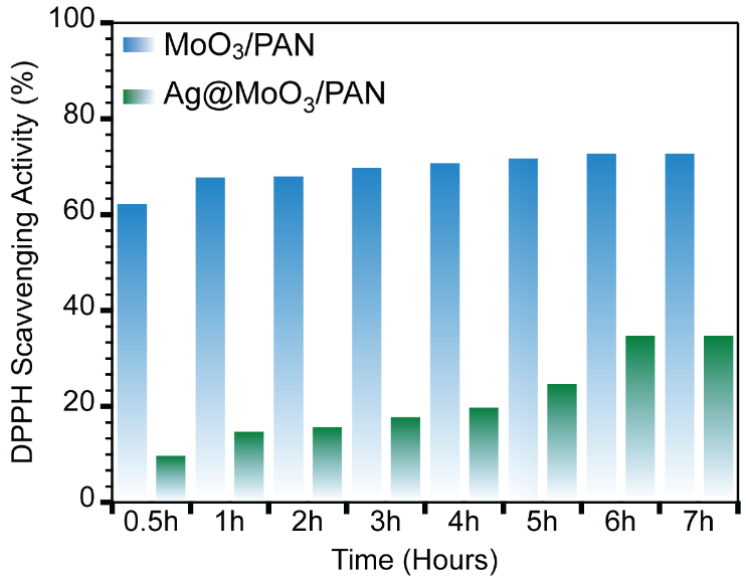

Figure 3—9: DPPH free radical scavenging activity of MoO_3/PAN composite membrane and silver doped composite membrane.

3.9 Antimicrobial assessments

Antibacterial were conducted using a method explained in our previous research[43]. To evaluate the antimicrobial properties of the produced fibers, we employed the agar disc diffusion assay following the standard test method (AATCC 147-1998). Specifically, bacterial strains, *Escherichia coli (E. coli)* and *Bacillus subtilis (B. subtilis)*, were utilized for the experiment. In this assay, we applied 25 µl of a 10^{-5} dilution of the bacterial strains onto sterile agar plates. Subsequently, two fiber samples were cut into 10 mm round shapes and gently positioned on the agar surface. Gentle pressure was applied to ensure close contact between the fibers and the agar. The plates were then incubated at 37°C for 20 hours. **Figure *3—10***a-c visually demonstrates the antibacterial activity of the MoO_3/PAN nanofiber membranes, as evidenced by the presence of inhibition zones on the corresponding agar plates. These inhibition zones serve as indicators of the membrane's efficacy in impeding the growth of both *Escherichia coli* and *Bacillus subtilis* bacteria. The mechanism underlying bacterial death is attributed to hydroxonium ions[33]. Initially, molybdenum trioxide (MoO_3) reacts with water to form molybdic acid (H_2MoO_4). Upon contact with water, molybdic acid releases hydroxonium ions (H_3O^+). These hydroxonium ions interact with the bacterial cell membrane, causing DNA damage, inhibiting the synthesis of new proteins, and ultimately resulting in cell destruction, as schematically demonstrated in **Figure *3—10***d. At equilibrium, hydroxonium ions are transformed back into molybdic acid[57].

The introduction of silver, referred to as "silver doping," further enhances the inhibition of bacterial viability, especially in the case of *Escherichia coli*. Ag^+ ions are released from the Ag@MoO_3/PAN membrane and interact with the cell membranes of both *E. coli* and *B. subtilis*, leading to the disruption of these bacterial cell membranes.

AgNPs exhibit antibacterial effects by binding to bacterial surfaces and subsequently penetrating the bacteria to modulate their activities by dephosphorylating tyrosine residues[13,58]. It is widely accepted that protein dephosphorylation can inhibit enzyme activity. When the activity of enzymes related to bacterial growth is inhibited, the behavior of the bacteria is disrupted or altered[59]. Concurrently, this interaction damages DNA and ribosomes, resulting in cell death, as illustrated in **Figure *3—10*e**. This effect is particularly pronounced in the case of *E. coli*, where the inhibition zone is larger for the Ag@MoO_3/PAN composite nanofiber membrane compared to the MoO_3/PAN composite nanofiber membrane.

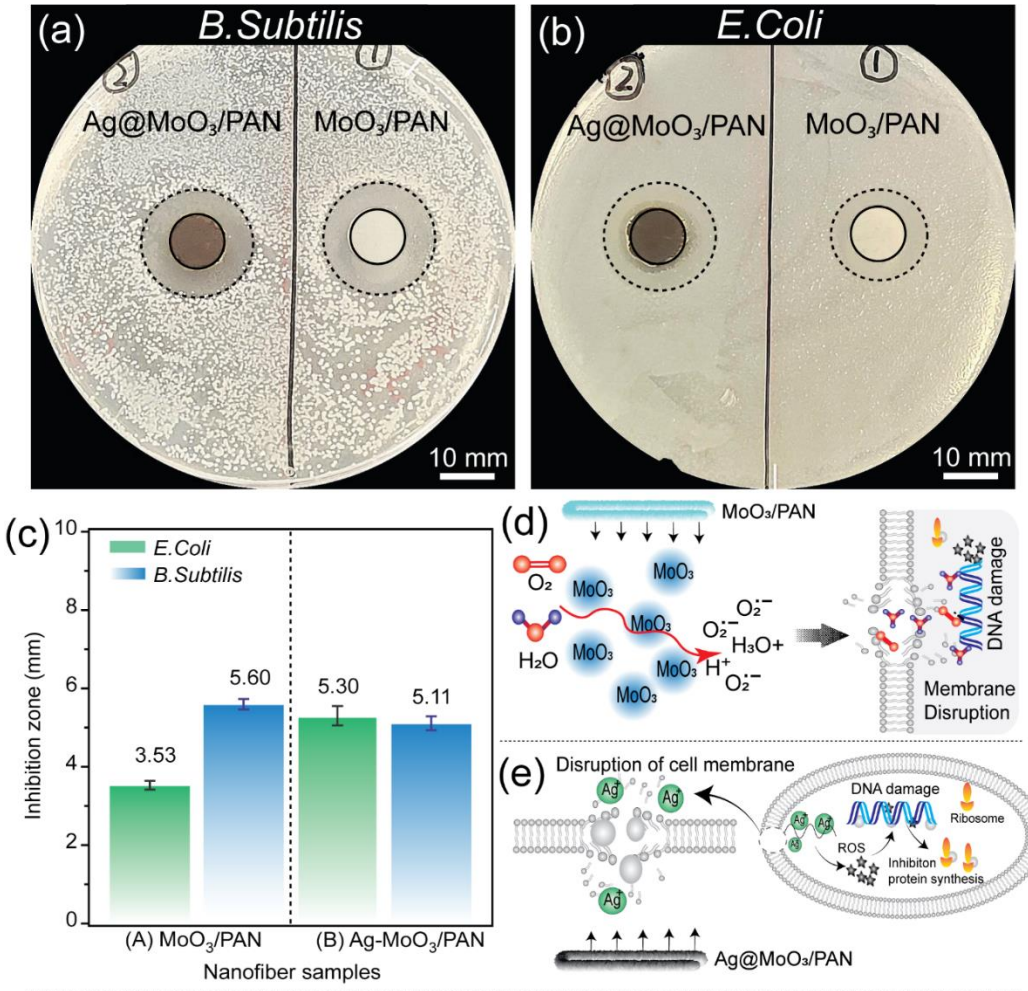

Figure 3—10: (a) *B. subtilis* Agar plates of antibacterial performance by inhibition zone

diameter (b) *E. Coli* agar plate (c) inhibition zone diameter of as prepared nanofiber membranes (d) schematic illustration of bacteria-killing behaviors of Ag@MoO_3/PAN and (e) schematic illustration of bacteria-killing behaviors by MoO_3/PAN composite nanofiber membrane.

3.10 Water contact angle (WCA)

WCA shows in **Figure *3—11***, with the MoO_3/PAN composite nanofiber membrane exhibiting contact angles of approximately 77°. These angles indicate the hydrophilic nature of the material, facilitating enhanced absorption of wound exudate[60]. This property helps maintain a moist wound environment, preventing the formation of a dry scab. Upon the introduction of silver into the MoO_3/PAN composite, the water contact angle decreases by 9%. This reduction can likely be attributed to the higher surface area of the membrane, as confirmed by our BET surface area measurements. Consequently, the Ag@MoO_3/PAN nanofiber membrane exhibits improved wettability, enhancing its ability to interact with liquids.

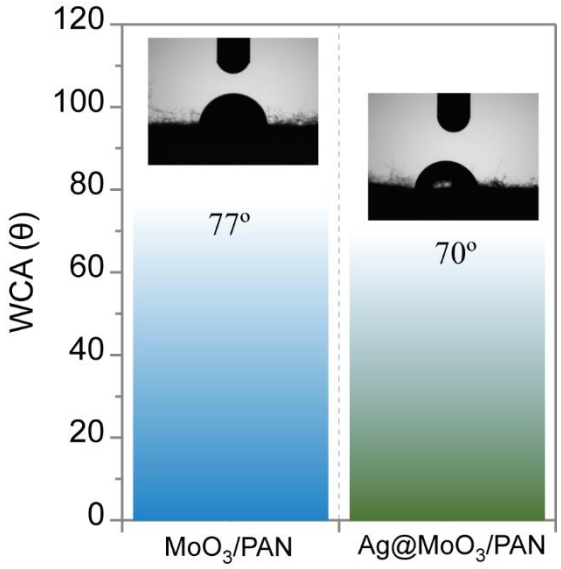

Figure 3—11: Water contact angle of as prepared MoO_3/PAN composite membrane and

silver dopped Ag@MoO_3/PAN membrane.

3.11 The release profile of Ag^+ ions

Release play a crucial role in determining the antibacterial activity of Ag-incorporated nanofiber membranes (NFMs)[12]. We conducted an evaluation to quantify the release rates and amounts of silver (in ppm) from Ag-MoO_3/PAN membranes, as illustrated in **Figure *3—12***a. To assess the release behavior across Ag-MoO_3/PAN samples, we employed inductively coupled plasma optical emission spectroscopy (ICP-OES) and prepared standard solutions with silver concentrations of 0.5, 1, 5, 10, and 20 ppm to establish a calibration curve. The coefficient factor R^2 was determined to be 0.999, as shown in **Figure *3—12***b. This procedure for measuring the release profile aligns with previous reports.

When it comes to traditional silver nanoparticles (AgNPs) and nanomaterials loaded with AgNPs, it's not easy to control how silver ions are released. So, how effective these materials are at killing bacteria often depends on how much they are exposed to in each situation. Initially having a lot of silver ions inside bacteria helps to get quickly and effectively rid of the bacteria and hinders microorganisms from being resistant against antibiotic materia[12,40]. After the initial burst, there must be control and maintenance of silver release are important, excessive silver will not damage the skin[61]. The release of these silver ions from materials containing AgNPs usually happens slowly or rapidly increases continuously[62]. This is why it's important to find ways to initially increase the amount of silver ions and then steadily maintain the release of ions.

The results indicate that the release of silver ions is controlled by the MoO_3/PAN composite membrane. These results show that initially, there is a rapid release of silver ions within the first 7 hours, followed by a significant decrease in the release rate after

one day. During the initial 7 hours, there is a continuous increase in silver ion release, reaching a peak of 31.95 ppm. However, after the initial burst, there is a noticeable reduction in the rate of silver ion release. At the end of the first day, the release was 10.71 ppm, which is a 33.56% reduction from the peak value. The release then remains relatively stable with minor fluctuations over the next seven days. This reduction in silver ion release rate after the initial burst could be attributed to the MoO_3/PAN composite membrane having functional groups that can interact with silver ions. These interactions can lead to the binding or complexation of silver ions on the membrane surface or within its structure[9,59]. This binding reduces the concentration of free silver ions available for release. Additionally, at the start, the membrane has many available binding sites for silver ions, but over time, these binding sites might be decreased, resulting in reduced release[41,43,63].

Furthermore, we analyzed the release data of the Ag@MoO_3/PAN composite membrane using different models, as described in a previous report[64]. The release data showed a better fit with the Peppas and first-order models, as shown in **Figure *3—12***c for hours and **Figure *3—12***d for days release, suggesting that multiple mechanisms may be involved in the release process. The Korsmeyer-Peppas model is a general approach used to describe the release of drugs and other substances[65].

$$F = kt^n \quad (2)$$

The drug, which is encapsulated within porous materials, can be described by the first-order equation[66].

$$F = 1 - e^{-kt} \quad (3)$$

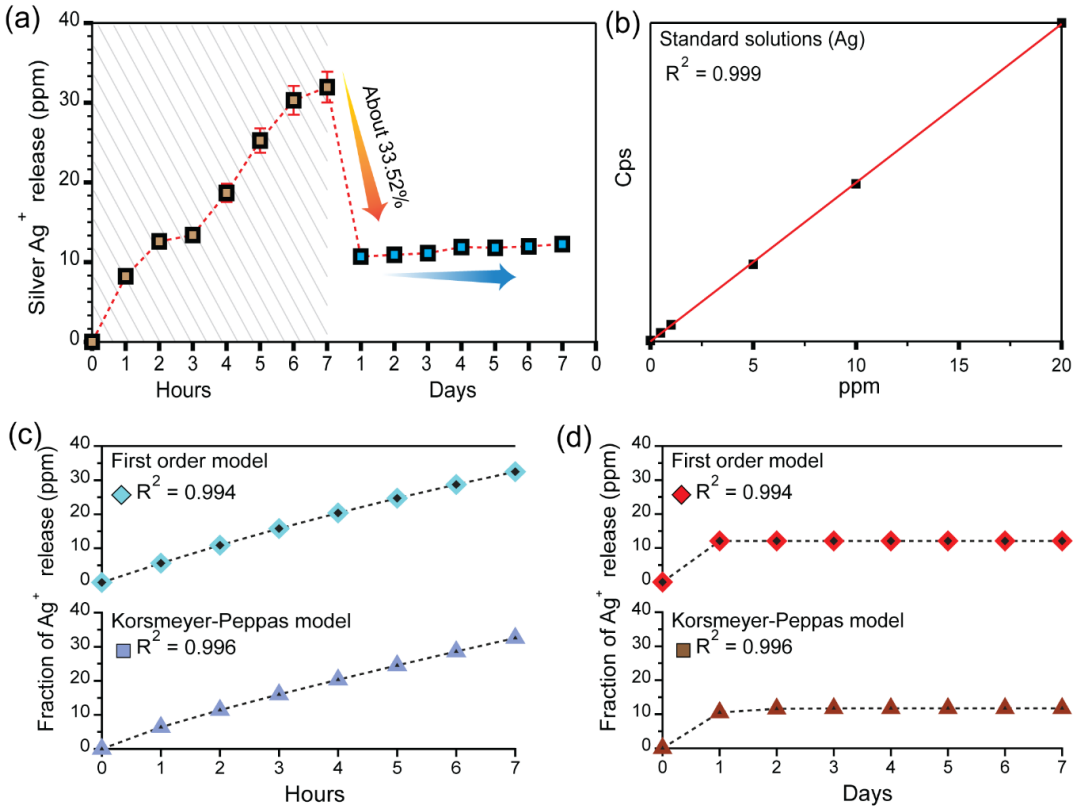

Figure 3—12: (a) silver release of Ag@MoO_3/PAN nanofiber membrane, (b) standard solution of Ag with different concentrations, (c), and (d) first order and Peppas model fitted curves of silver release data of hours and days respectively.

3.12 Conclusion

In summary, we have successfully synthesized a hybrid composite material comprising molybdenum oxide and polyacrylonitrile (MoO_3/PAN) through electrospinning. Additionally, we have developed a rapid green synthesis method that can reduce silver ions to metallic silver on the surface of the composite material within one minute, resulting in the formation of an Ag@MoO_3/PAN membrane. Our research has confirmed that molybdenum oxide exhibits highly effective antimicrobial activity against both *Escherichia coli* and *Bacillus subtilis* bacteria. Furthermore, the incorporation of silver nanoparticles into the composite material has enhanced its antibacterial properties, particularly against *Escherichia coli* bacteria. Moreover, we have increased the surface area of the molybdenum composite material by 25.89% through the incorporation of silver nanoparticles, leading to a 9% improvement in surface wettability. We have also addressed the issue of uncontrolled silver release by this new composite hybrid material of MoO_3/PAN, reducing the excessive release of silver ions by 33.52% within 24 hours. This intelligent hybrid material, Ag@MoO_3/PAN, has also proven effective in combating multidrug-resistant bacterial strains. We firmly believe that this study opens possibilities for extensive research, not only in the field of antimicrobial activity but also in other applications, such as water filtration and the use of MoO_3/PAN membranes as surface-enhanced Raman spectroscopy (SERS) substrates. These applications can be further optimized by controlling the morphology of the materials.

References:

(1) Santos, F. G.; Bonkovoski, L. C.; Garcia, F. P.; Cellet, T. S. P.; Witt, M. A.; Nakamura, C. V.; Rubira, A. F.; Muniz, E. C. Antibacterial Performance of a PCL-PDMAEMA Blend Nanofiber-Based Scaffold Enhanced with Immobilized Silver Nanoparticles. *ACS Appl. Mater. Interfaces* **2017**, *9* (11), 9304–9314. https://doi.org/10.1021/acsami.6b14411.

(2) Dreifke, M. B.; Jayasuriya, A. A.; Jayasuriya, A. C. Current Wound Healing Procedures and Potential Care. *Mater. Sci. Eng. C* **2015**, *48*, 651–662. https://doi.org/10.1016/j.msec.2014.12.068.

(3) Mulani, M. S.; Kamble, E. E.; Kumkar, S. N.; Tawre, M. S.; Pardesi, K. R. Emerging Strategies to Combat ESKAPE Pathogens in the Era of Antimicrobial Resistance: A Review. *Front. Microbiol.* **2019**, *10*, 539. https://doi.org/10.3389/fmicb.2019.00539.

(4) De Oliveira, D. M. P.; Forde, B. M.; Kidd, T. J.; Harris, P. N. A.; Schembri, M. A.; Beatson, S. A.; Paterson, D. L.; Walker, M. J. Antimicrobial Resistance in ESKAPE Pathogens. *Clin. Microbiol. Rev.* **2020**, *33* (3). https://doi.org/10.1128/CMR.00181-19.

(5) Mancuso, G.; Midiri, A.; Gerace, E.; Biondo, C. Bacterial Antibiotic Resistance: The Most Critical Pathogens. *Pathog. (Basel, Switzerland)* **2021**, *10* (10). https://doi.org/10.3390/pathogens10101310.

(6) de Kraker, M. E. A.; Stewardson, A. J.; Harbarth, S. Will 10 Million People Die a Year Due to Antimicrobial Resistance by 2050? *PLoS Med.* **2016**, *13* (11), 1–6. https://doi.org/10.1371/journal.pmed.1002184.

(7) Frei, A.; Verderosa, A. D.; Elliott, A. G.; Zuegg, J.; Blaskovich, M. A. T. Metals to Combat Antimicrobial Resistance. *Nat. Rev. Chem.* **2023**, *7* (3), 202–224. https://doi.org/10.1038/s41570-023-00463-4.

(8) Jia, B.; Li, G.; Cao, E.; Luo, J.; Zhao, X.; Huang, H. Recent Progress of Antibacterial Hydrogels in Wound Dressings. *Mater. Today Bio* **2023**, *19* (January), 100582. https://doi.org/10.1016/j.mtbio.2023.100582.

(9) Liao, J.; Wang, L.; Ding, S.; Tian, G.; Hu, H.; Wang, Q.; Yin, W. Molybdenum-Based Antimicrobial Nanomaterials: A Comprehensive Review. *Nano Today* **2023**, *50*, 101875. https://doi.org/10.1016/j.nantod.2023.101875.

(10) Zhou, Z.; Li, B.; Liu, X.; Li, Z.; Zhu, S.; Liang, Y.; Cui, Z.; Wu, S. Recent Progress in Photocatalytic Antibacterial. *ACS Appl. Bio Mater.* **2021**, *4* (5), 3909–3936. https://doi.org/10.1021/acsabm.0c01335.

(11) Serag, E.; El-Aziz, A. M. A.; El-Maghraby, A.; Taha, N. A. Electrospun Non-Wovens Potential Wound Dressing Material Based on Polyacrylonitrile/Chicken Feathers Keratin Nanofiber. *Sci. Rep.* **2022**, *12* (1), 15460. https://doi.org/10.1038/s41598-022-19390-3.

(12) Xu, Z.; Zhang, C.; Wang, X.; Liu, D. Release Strategies of Silver Ions from Materials for Bacterial Killing. *ACS Appl. Bio Mater.* **2021**, *4* (5), 3985–3999. https://doi.org/10.1021/acsabm.0c01485.

(13) Xu, F.; Piett, C.; Farkas, S.; Qazzaz, M.; Syed, N. I. Silver Nanoparticles (AgNPs) Cause Degeneration of Cytoskeleton and Disrupt Synaptic Machinery of Cultured Cortical Neurons. *Mol. Brain* **2013**, *6* (1), 1–15. https://doi.org/10.1186/1756-6606-6-29.

(14) Wang, C.; Wang, W.; Zhang, L.; Zhong, S.; Yu, D. Electrospinning of PAN/Ag

NPs Nanofiber Membrane with Antibacterial Properties. *J. Mater. Res.* **2019**, *34* (10), 1669–1677. https://doi.org/10.1557/jmr.2019.44.

(15) Elhassan, E.; Devnarain, N.; Mohammed, M.; Govender, T.; Omolo, C. A. Engineering Hybrid Nanosystems for Efficient and Targeted Delivery against Bacterial Infections. *J. Control. release Off. J. Control. Release Soc.* **2022**, *351*, 598–622. https://doi.org/10.1016/j.jconrel.2022.09.052.

(16) Jayakumar, A.; Mathew, S.; Radoor, S.; Kim, J. T.; Rhim, J. W.; Siengchin, S. Recent Advances in Two-Dimensional Nanomaterials: Properties, Antimicrobial, and Drug Delivery Application of Nanocomposites. *Mater. Today Chem.* **2023**, *30*, 101492. https://doi.org/10.1016/j.mtchem.2023.101492.

(17) Guggenbichler, J.K., Eberhardt, N., Martinez, H.P., Wildner, H. Substance with an Antimicrobial Effect. PCT/EP2007/009814, **2007**.

(18) Stan, D.; Enciu, A.-M.; Mateescu, A. L.; Ion, A. C.; Brezeanu, A. C.; Stan, D.; Tanase, C. Natural Compounds With Antimicrobial and Antiviral Effect and Nanocarriers Used for Their Transportation. *Front. Pharmacol.* **2021**, *12*, 723233. https://doi.org/10.3389/fphar.2021.723233.

(19) Rabiee, N.; Ahmadi, S.; Akhavan, O.; Luque, R. Silver and Gold Nanoparticles for Antimicrobial Purposes against Multi-Drug Resistance Bacteria. *Mater. (Basel, Switzerland)* **2022**, *15* (5). https://doi.org/10.3390/ma15051799.

(20) Rodríguez-León, E.; Rodríguez-Vázquez, B. E.; Martínez-Higuera, A.; Rodríguez-Beas, C.; Larios-Rodríguez, E.; Navarro, R. E.; López-Esparza, R.; Iñiguez-Palomares, R. A. Synthesis of Gold Nanoparticles Using Mimosa Tenuiflora Extract, Assessments of Cytotoxicity, Cellular Uptake, and Catalysis. *Nanoscale Res. Lett.* **2019**, *14* (1), 334. https://doi.org/10.1186/s11671-019-3158-

9.

(21) Zhang, S.; Tang, Y.; Vlahovic, B. A Review on Preparation and Applications of Silver-Containing Nanofibers. *Nanoscale Res. Lett.* **2016**, *11* (1), 1–8. https://doi.org/10.1186/s11671-016-1286-z.

(22) Husanu, E.; Chiappe, C.; Bernardini, A.; Cappello, V.; Gemmi, M. Synthesis of Colloidal Ag Nanoparticles with Citrate Based Ionic Liquids as Reducing and Capping Agents. *Colloids Surfaces A Physicochem. Eng. Asp.* **2018**, *538*, 506–512. https://doi.org/10.1016/j.colsurfa.2017.11.033.

(23) Mishra, A.; Djoko, K. Y.; Lee, Y. H.; Lord, R. M.; Kaul, G.; Akhir, A.; Saxena, D.; Chopra, S.; Walton, J. W. Water-Soluble Copper Pyrithione Complexes with Cytotoxic and Antibacterial Activity. *Org. Biomol. Chem.* **2023**, *21* (12), 2539–2544. https://doi.org/10.1039/d2ob01224c.

(24) Khandelwal, M.; Kumawat, A.; Misra, K. P.; Khangarot, R. K. Efficient Antibacterial Activity in Copper Oxide Nanoparticles Biosynthesized via Jasminum Sambac Flower Extract. *Part. Sci. Technol.* **2023**, *41* (5), 640–652. https://doi.org/10.1080/02726351.2022.2129117.

(25) Wang, Q.; Wang, H.; Zhang, T.; Hu, Z.; Xia, L.; Li, L.; Chen, J.; Jiang, S. Antibacterial Activity of Polyvinyl Alcohol/WO3Films Assisted by Near-Infrared Light and Its Application in Freshness Monitoring. *J. Agric. Food Chem.* **2021**, *69* (3), 1068–1078. https://doi.org/10.1021/acs.jafc.0c06961.

(26) Mustafa, Y. F. Modern Developments in the Application and Function of Metal/Metal Oxide Nanocomposite–Based Antibacterial Agents. *Bionanoscience* **2023**, *13* (2), 840–852. https://doi.org/10.1007/s12668-023-01100-6.

(27) Xin, Q.; Shah, H.; Nawaz, A.; Xie, W.; Akram, M. Z.; Batool, A.; Tian, L.; Jan,

S. U.; Boddula, R.; Guo, B.; Liu, Q.; Gong, J. R. Antibacterial Carbon-Based Nanomaterials. *Adv. Mater.* **2019**, *31* (45), 1–15. https://doi.org/10.1002/adma.201804838.

(28) Yuan, H.; Chen, L.; Hong, F. F. A Biodegradable Antibacterial Nanocomposite Based on Oxidized Bacterial Nanocellulose for Rapid Hemostasis and Wound Healing. *ACS Appl. Mater. Interfaces* **2020**, *12* (3), 3382–3392. https://doi.org/10.1021/acsami.9b17732.

(29) Cao, W.; Yue, L.; Wang, Z. High Antibacterial Activity of Chitosan – Molybdenum Disulfide Nanocomposite. *Carbohydr. Polym.* **2019**, *215* (February), 226–234. https://doi.org/10.1016/j.carbpol.2019.03.085.

(30) Drobot, N. F.; Noskova, O. A.; Ovchinnikova, N. A.; Zvereva, G. A.; Larin, G. M.; Krenev, V. A.; Trifonova, E. N.; Drobot, D. V. Complex Formation during Molybdenum Chlorination in DMF Medium. *Russ. J. Coord. Chem. Khimiya* **2003**, *29* (7), 474–477. https://doi.org/10.1023/A:1024774829021.

(31) Fakhri, A.; Nejad, P. A. Antimicrobial, Antioxidant and Cytotoxic Effect of Molybdenum Trioxide Nanoparticles and Application of This for Degradation of Ketamine under Different Light Illumination. *J. Photochem. Photobiol. B Biol.* **2016**, *159*, 211–217. https://doi.org/10.1016/j.jphotobiol.2016.04.002.

(32) Akhtar, M. J.; Ahamed, M.; Alhadlaq, H. A.; Alshamsan, A.; Majeed Khan, M. A.; Alrokayan, S. A. Antioxidative and Cytoprotective Response Elicited by Molybdenum Nanoparticles in Human Cells. *J. Colloid Interface Sci.* **2015**, *457*, 370–377. https://doi.org/10.1016/j.jcis.2015.07.034.

(33) Zollfrank, C.; Gutbrod, K.; Wechsler, P.; Guggenbichler, J. P. Antimicrobial Activity of Transition Metal Acid MoO3 Prevents Microbial Growth on Material

Surfaces. *Mater. Sci. Eng. C* **2012**, *32* (1), 47–54. https://doi.org/10.1016/j.msec.2011.09.010.

(34) Xing, Y.; Cai, Y.; Cheng, J.; Xu, X. Applications of Molybdenum Oxide Nanomaterials in the Synergistic Diagnosis and Treatment of Tumor. *Appl. Nanosci.* **2020**, *10* (7), 2069–2083. https://doi.org/10.1007/s13204-020-01389-9.

(35) Desai, N.; Mali, S. Chemically Grown MoO3 Nanorods for Antibacterial Activity Study. *J. Nanomed. Nanotechnol.* **2015**, *06* (06). https://doi.org/10.4172/2157-7439.1000338.

(36) De Foggi, C. C.; De Oliveira, R. C.; Assis, M.; Fabbro, M. T.; Mastelaro, V. R.; Vergani, C. E.; Gracia, L.; Andrés, J.; Longo, E.; Machado, A. L. Unvealing the Role of β-Ag2MoO4 Microcrystals to the Improvement of Antibacterial Activity. *Mater. Sci. Eng. C* **2020**, *111* (September 2018), 110765. https://doi.org/10.1016/j.msec.2020.110765.

(37) Huang, F.; Gao, Y.; Zhang, Y.; Cheng, T.; Ou, H.; Yang, L.; Liu, J.; Shi, L.; Liu, J. Silver-Decorated Polymeric Micelles Combined with Curcumin for Enhanced Antibacterial Activity. *ACS Appl. Mater. Interfaces* **2017**, *9* (20), 16880–16889. https://doi.org/10.1021/acsami.7b03347.

(38) Wang, J.; Li, T.; Yan, T.; Wei, X.; Qu, X.; Yuan, S. Friction Behavior of Silver Perrhenate in Oil as Lubricating Additive for Use at Elevated Temperatures. *Mater. (Basel, Switzerland)* **2019**, *12* (13). https://doi.org/10.3390/ma12132199.

(39) Niu, Z.; Zhou, C.; Wang, J.; Xu, Y.; Gu, C.; Jiang, T.; Zeng, S.; Zhang, Y.; Ang, D. S.; Zhou, J. UV-Light-Assisted Preparation of MoO3−x/Ag NPs Film and Investigation on the SERS Performance. *J. Mater. Sci.* **2020**, *55* (21), 8868–8880. https://doi.org/10.1007/s10853-020-04669-5.

(40) Dobias, J.; Bernier-Latmani, R. Silver Release from Silver Nanoparticles in Natural Waters. *Environ. Sci. Technol.* **2013**, *47* (9), 4140–4146. https://doi.org/10.1021/es304023p.

(41) Shao, P.; Chang, Z.; Li, M.; Lu, X.; Jiang, W.; Zhang, K.; Luo, X.; Yang, L. Mixed-Valence Molybdenum Oxide as a Recyclable Sorbent for Silver Removal and Recovery from Wastewater. *Nat. Commun.* **2023**, *14* (1), 1365. https://doi.org/10.1038/s41467-023-37143-2.

(42) Kim, T. I.; Kwon, B.; Yoon, J.; Park, I. J.; Bang, G. S.; Park, Y. K.; Seo, Y. S.; Choi, S. Y. Antibacterial Activities of Graphene Oxide-Molybdenum Disulfide Nanocomposite Films. *ACS Appl. Mater. Interfaces* **2017**, *9* (9), 7908–7917. https://doi.org/10.1021/acsami.6b12464.

(43) Farooq, M.; Khalid, M.; Yoshinori, Y.; Wang, F.; Iqbal, M. A.; Sarwar, M. N.; Mayakrishnan, G.; Kim, I. S. Ag and MoO 3 Nanoparticle-Containing Polyacrylonitrile Nanofiber Membranes for Wound Dressings. **2023**. https://doi.org/10.1021/acsanm.3c03435.

(44) Wei, J.; Jiao, X.; Wang, T.; Chen, D. Electrospun Photochromic Hybrid Membranes for Flexible Rewritable Media. *ACS Appl. Mater. Interfaces* **2016**, *8* (43), 29713–29720. https://doi.org/10.1021/acsami.6b10620.

(45) He, J.-H.; Wan, Y.-Q.; Yu, J.-Y. Effect of Concentration on Electrospun Polyacrylonitrile (PAN) Nanofibers. *Fibers Polym.* **2008**, *9* (2), 140–142. https://doi.org/10.1007/s12221-008-0023-3.

(46) Oliveira, C. A.; Volanti, D. P.; Nogueira, A. E.; Zamperini, C. A.; Vergani, C. E.; Longo, E. Well-Designed β-Ag2MoO4 Crystals with Photocatalytic and Antibacterial Activity. *Mater. Des.* **2017**, *115*, 73–81.

https://doi.org/10.1016/j.matdes.2016.11.032.

(47) Fleisch, T. H.; Mains, G. J. An XPS Study of the UV Reduction and Photochromism of MoO3 and WO3. *J. Chem. Phys.* **1982**, *76* (2), 780–786. https://doi.org/10.1063/1.443047.

(48) Chang, L.; Duan, L.; Sheng, M.; Yuan, J.; Yi, H.; Zou, Y.; Uddin, A. Optimising Non-Patterned MoO3/Ag/MoO3 Anode for High-Performance Semi-Transparent Organic Solar Cells towards Window Applications. *Nanomaterials*. **2020**. https://doi.org/10.3390/nano10091759.

(49) Shafaei, S.; Dörrstein, J.; Guggenbichler, J. P.; Zollfrank, C. Cellulose Acetate-Based Composites with Antimicrobial Properties from Embedded Molybdenum Trioxide Particles. *Lett. Appl. Microbiol.* **2017**, *64* (1), 43–50. https://doi.org/10.1111/lam.12670.

(50) Walton, K. S.; Snurr, R. Q. Applicability of the BET Method for Determining Surface Areas of Microporous Metal-Organic Frameworks. *J. Am. Chem. Soc.* **2007**, *129* (27), 8552–8556. https://doi.org/10.1021/ja071174k.

(51) Lee, J.; Kim, J. G.; Chang, J. Y. Fabrication of a Conjugated Microporous Polymer Membrane and Its Application for Membrane Catalysis. *Sci. Rep.* **2017**, *7* (1), 13568. https://doi.org/10.1038/s41598-017-13827-w.

(52) Ullah, A.; Saito, Y.; Ullah, S.; Haider, M. K.; Nawaz, H.; Duy-Nam, P.; Kharaghani, D.; Kim, I. S. Bioactive Sambong Oil-Loaded Electrospun Cellulose Acetate Nanofibers: Preparation, Characterization, and in-Vitro Biocompatibility. *Int. J. Biol. Macromol.* **2021**, *166*, 1009–1021. https://doi.org/10.1016/j.ijbiomac.2020.10.257.

(53) Alam, M. W.; BaQais, A.; Mir, T. A.; Nahvi, I.; Zaidi, N.; Yasin, A. Effect of

Mo Doping in NiO Nanoparticles for Structural Modification and Its Efficiency for Antioxidant, Antibacterial Applications. *Sci. Rep.* **2023**, *13* (1), 1–17. https://doi.org/10.1038/s41598-023-28356-y.

(54) Özyürek, M.; Güngör, N.; Baki, S.; Güçlü, K.; Apak, R. Development of a Silver Nanoparticle-Based Method for the Antioxidant Capacity Measurement of Polyphenols. *Anal. Chem.* **2012**, *84* (18), 8052–8059. https://doi.org/10.1021/ac301925b.

(55) Sudha, A.; Jeyakanthan, J.; Srinivasan, P. Green Synthesis of Silver Nanoparticles Using Lippia Nodiflora Aerial Extract and Evaluation of Their Antioxidant, Antibacterial and Cytotoxic Effects. *Resour. Technol.* **2017**, *3* (4), 506–515. https://doi.org/https://doi.org/10.1016/j.reffit.2017.07.002.

(56) Patil, S.; Rajiv, P.; Sivaraj, R. AN INVESTIGATION OF ANTIOXIDANT AND CYTOTOXIC PROPERTIES OF GREEN SYNTHESIZED SILVER NANOPARTICLES; 2015.

(57) Sharma, A.; Saini, A. K.; Kumar, N.; Tejwan, N.; Singh, T. A.; Thakur, V. K.; Das, J. Methods of Preparation of Metal-Doped and Hybrid Tungsten Oxide Nanoparticles for Anticancer, Antibacterial, and Biosensing Applications. *Surfaces and Interfaces* **2022**, *28* (July 2021), 101641. https://doi.org/10.1016/j.surfin.2021.101641.

(58) Mikhailova, E. O. Silver Nanoparticles: Mechanism of Action and Probable Bio-Application. *J. Funct. Biomater.* **2020**, *11* (4). https://doi.org/10.3390/jfb11040084.

(59) Tanasic, D.; Rathner, A.; Kollender, J. P.; Rathner, P.; Müller, N.; Zelenka, K. C.; Hassel, A. W.; Mardare, C. C. Silver-, Calcium-, and Copper Molybdate

Compounds: Preparation, Antibacterial Activity, and Mechanisms. *Biointerphases* **2017**, *12* (5). https://doi.org/10.1116/1.4996434.

(60) Song, M.; Zhao, Q.; Wang, X.; Shi, C.; Hu, X.; Li, J. A Hydrophilic/Hydrophobic Janus Membrane Used as Wound Dressings with Enhanced Antibacterial Properties. *Fibers Polym.* **2022**, *23* (9), 2511–2516. https://doi.org/10.1007/s12221-022-0127-1.

(61) Wang, L.; Hu, C.; Shao, L. The Antimicrobial Activity of Nanoparticles: Present Situation and Prospects for the Future. *Int. J. Nanomedicine* **2017**, *12*, 1227–1249. https://doi.org/10.2147/IJN.S121956.

(62) Wang, X.; Herting, G.; Odnevall Wallinder, I.; Blomberg, E. Adsorption of Lysozyme on Silver and Its Influence on Silver Release. *Langmuir* **2014**, *30* (46), 13877–13889. https://doi.org/10.1021/la503170x.

(63) Wang, Z.; Zhu, J.; Chen, L.; Deng, K.; Huang, H. Multifunctional Gold-Silver-Carbon Quantum Dots Nano-Hybrid Composite: Advancing Antibacterial Wound Healing and Cell Proliferation. *ACS Appl. Mater. Interfaces* **2023**, *15* (34), 40241–40254. https://doi.org/10.1021/acsami.3c07625.

(64) Jatoi, A. W.; Jo, Y. K.; Lee, H.; Oh, S. G.; Hwang, D. S.; Khatri, Z.; Cha, H. J.; Kim, I. S. Antibacterial Efficacy of Poly(Vinyl Alcohol) Composite Nanofibers Embedded with Silver-Anchored Silica Nanoparticles. *J. Biomed. Mater. Res. - Part B Appl. Biomater.* **2018**, *106* (3), 1121–1128. https://doi.org/10.1002/jbm.b.33925.

(65) Phan, D. N.; Dorjjugder, N.; Saito, Y.; Taguchi, G.; Ullah, A.; Kharaghani, D.; Kim, I. S. The Synthesis of Silver-Nanoparticle-Anchored Electrospun Polyacrylonitrile Nanofibers and a Comparison with as-Spun

Silver/Polyacrylonitrile Nanocomposite Membranes upon Antibacterial Activity. *Polym. Bull.* **2020**, *77* (8), 4197–4212. https://doi.org/10.1007/s00289-019-02969-8.

(66) Lu, D. R.; Abu-Izza, K.; Mao, F. Nonlinear Data Fitting for Controlled Release Devices: An Integrated Computer Program. *Int. J. Pharm.* **1996**, *129* (1–2), 243–251. https://doi.org/10.1016/0378-5173(95)04356-X.

CHAPTER 4. Conclusion

In this comprehensive conclusion, we synthesize the key findings and implications from each of the chapters in the thesis focused on wound care applications:

Chapter 1 provides an overview of the fundamental context surrounding the synthesis of polymers through electrospinning, as well as the application of silver and Mo-based dressings in wound treatment. The study is presented through an analysis of existing literature data.

Chapter 2: In this chapter, the focus was on understanding how different reducing agents (NaOH, $NaBH_4$, sodium citrate, and UV light) could modify molybdenum incorporated MoO_3/PAN nanofiber membranes for wound care application. The subsequent treatment of these nanofibers with different reducing agents offered a crucial insight into their potential applications in wound dressing. Notably, the NaOH-treated sample exhibited a hydrophobic surface, making it suitable for wounds that require a drier healing environment, while $NaBH_4$ treatment enhanced fluid absorption, catering to wounds with moderate exudate levels. Furthermore, the chapter emphasized the impressive antibacterial activity of all treated samples against both *E. coli* and *B. subtilis*, offering diverse options for wound care depending on specific patient needs.

Chapter 3: First time our study successfully created a hybrid composite material by combining molybdenum oxide and polyacrylonitrile (MoO_3/PAN) using electrospinning. Additionally, we devised an efficient and eco-friendly method for rapidly reducing silver ions to form metallic silver on the composite material's surface within one minute. Later the development of Ag@MoO_3/PAN membranes, a hybrid composite material incorporating silver nanoparticles into molybdenum oxide/polyacrylonitrile membrane. This material demonstrated effective antimicrobial properties against both *E. coli* and *B. subtilis*. What makes this hybrid material stand out is its solution to the problem of

uncontrolled silver ion release, making it safer for wound care applications by reducing the excessive release of silver ions by 33.52% within 24 hours. Moreover, we have increased the surface area of the molybdenum composite material by 25.89% through the incorporation of silver nanoparticles, leading to a 9% improvement in surface wettability.

CHAPTER 5. Perspective

The research presented in this thesis offers several promising perspectives for further exploration:

Advanced Wound Care Materials: The findings from this research open doors to the development of more advanced wound care materials. By customizing materials to specific wound conditions and incorporating controlled release of antibacterial agents, these materials could significantly improve the healing process for patients with a variety of wounds.

Multidrug-Resistant Infection Control: The research's success in combating multidrug-resistant bacterial strains is crucial. It offers hope in the fight against increasingly resistant pathogens. Further research could explore the potential use of these materials in various medical settings to control hospital-acquired infections.

Broader Healthcare Applications: Beyond wound care, the hybrid materials developed could find applications in other areas of healthcare. The potential for water filtration, medical devices, and even diagnostic tools like surface-enhanced Raman spectroscopy (SERS) substrates presents exciting opportunities.

Eco-Friendly Synthesis Methods: The development of eco-friendly synthesis methods, as seen in the rapid green synthesis of Ag@MoO_3/PAN, aligns with the growing need for sustainable and environmentally friendly technologies. These methods can be applied in various fields beyond wound care.

Material Morphology Control: The study highlights the importance of material morphology in enhancing properties like surface wettability. Future research can explore ways to fine-tune material morphology to optimize performance in different applications.

Interdisciplinary Research: The research bridges materials science,

nanotechnology, and healthcare. It encourages interdisciplinary collaboration among scientists, engineers, and healthcare professionals to further advance the field.

Acknowledgement

I would like to express the utmost gratitude to my supervisor, Professor KIM Ick Soo for his invaluable advice, helpful discussions, suggestions, and continuous encouragement. I extend my gratitude to Professor Wataru Sugimoto for his numerous constructive pieces of advice, kind discussions, and encouragement. Without the enlightening guidance from Professor Wataru Sugimoto and Professor KIM Ick Soo, I could not have found the appropriate road in my academic career. My profound gratitude goes to Professor Hideaki Morikawa for his advice and encouragement. I am very thankful to Professor Yasushi Murakami, my tutor for four years, for his guidance and precious advice in helping me accomplish my goal.

I wish to thank Associate professor Tomoko Hashimoto from Department of Applied Biological Sciences Shinshu University for her helpful experimental assistance and insightful discussion. I am deeply thankful to Dr. Imran Muhammad from Clean Energy Research Center, Yamanashi University for his fruitful advice, helpful discussions, suggestions, and encouragement. I also extend my gratitude to Specially Appointed Associate Professor Gopiraman Mayakrishnan from Division of Molecules and Polymers, Interdisciplinary Cluster for Cutting Edge Research (ICCER), Institute for Fiber Engineering (IFES) for his helpful discussions and suggestions.

The financial support provided by the Japan Student Services Organization (JASSO) as a Monbukagakusho Honors Scholarship, and the salary support, travel expenses, and research incentives granted by the Next Generation (SPRING) program of JST, are greatly appreciated and acknowledged.

I also want to express my gratitude to my seniors, Dr. Azeem Ullah, Mr. Ryota Saito, my colleagues Md Kaiser Haider, Maira Khalid, Asim Iqbal, and Feifei Wang. Special thanks go to my collaborators; Yabuta Yoshinori, Muhammad Nauman Sarwar, Yuki Makiuchi, Emi Takamatsu, and Masaki Watanabe. This thesis could not have been completed without their earnest experiments and discussions. I would like to thank all the Gakumu Staff, especially Yukari Katayama for their patience and attention.

Finally, I thank my parents, Abdul Sattar and Sitaran Bibi for their financial support, everlasting understanding, and love.

Muhammad Farooq